Article

Immunity

# Transfer of cGAMP into Bystander Cells via LRRC8 Volume-Regulated Anion Channels Augments STING-Mediated Interferon Responses and Anti-viral Immunity

## Graphical Abstract

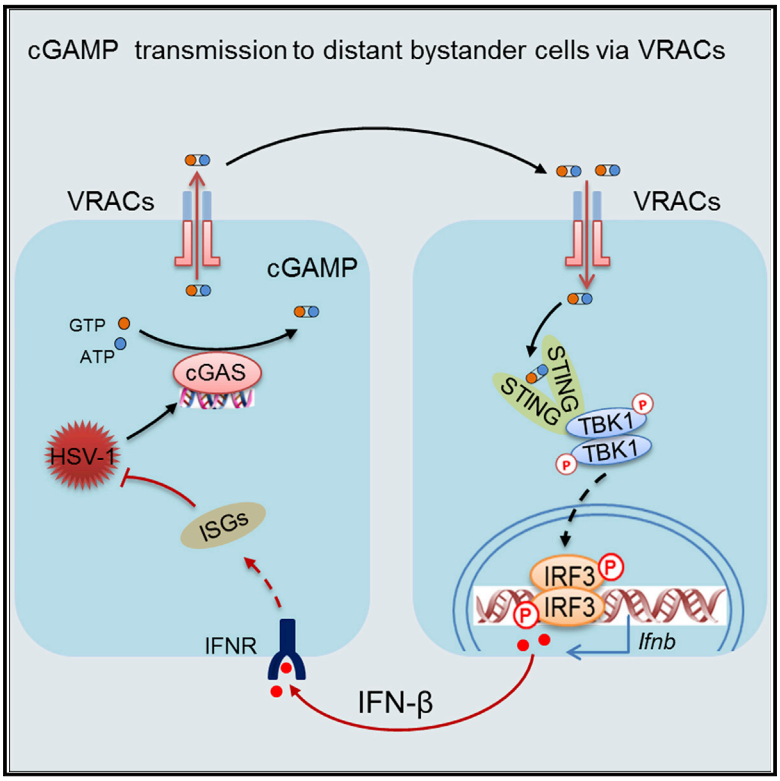


## Authors

Chun Zhou, Xia Chen, Rosa Planells-Cases, ..., Zhaozhu Qiu, Thomas J. Jentsch, Hui Xiao

## Correspondence

zhaozhu@jhmi.edu (Z.Q.), jentsch@fmp-berlin.de (T.J.J.), huixiao@ips.ac.cn (H.X.)

## In Brief

The second messenger cGAMP, produced by the enzyme cGAS upon sensing of cytosolic DNA in infected or malignant cells, can activate STING in bystander cells. Zhou et al. reveal that LRRC8 volume-regulated anion channels are important conduits of cGAMP in cell-to-cell transmission and are central to effective anti-viral immunity.

## Highlights

- LRRC8 volume-regulated anion channels function as a conduit for cGAMP efflux and influx
- Inflammatory factors intimately associated with viral infections activate LRRC8/VRAC channels
- LRRC8A/E VRACs play a crucial role in host defense against DNA viruses such as HSV-1
- The cGAMP-STING signaling in bystander cells contributes to the host IFN responses

Zhou et al., 2020, Immunity *52*, 767–781
May 19, 2020 
https://doi.org/10.1016/j.immuni.2020.03.016

CellPress

Immunity

CellPress

Article

# Transfer of cGAMP into Bystander Cells via LRRC8 Volume-Regulated Anion Channels Augments STING-Mediated Interferon Responses and Anti-viral Immunity

Chun Zhou,[1,15] Xia Chen,[1,2,15] Rosa Planells-Cases,[3,15] Jiachen Chu,[4] Li Wang,[1] Limin Cao,[1] Zhihong Li,[5,6] Karen I. López-Cayuqueo,[3] Yadong Xie,[1] Shiwei Ye,[7] Xiang Wang,[8] Florian Ullrich,[3] Shixin Ma,[1] Yiyuan Fang,[8] Xiaoming Zhang,[8] Zhikang Qian,[8] Xiaozheng Liang,[8] Shi-Qing Cai,[7] Zhengfan Jiang,[9] Dongming Zhou,[8] Qibin Leng,[10] Tsan S. Xiao,[11] Ke Lan,[12] Jinbo Yang,[2] Huabin Li,[13] Chao Peng,[5,6] Zhaozhu Qiu,[4,*] Thomas J. Jentsch,[3,14,*] and Hui Xiao[1,16,*]

[1]The Center for Microbes, Development and Health, CAS Key Laboratory of Molecular Virology & Immunology, Institut Pasteur of Shanghai, CAS Center for Excellence in Molecular Cell Science, University of Chinese Academy of Sciences, Chinese Academy of Sciences, Shanghai 200031, China
[2]College of Life Sciences, Lanzhou University, Lanzhou, Gansu 730000, China
[3]Leibniz-Forschungsinstitut für Molekulare Pharmakologie (FMP) and Max-Delbrück-Centrum für Molekulare Medizin, D-13125 Berlin, Germany
[4]Department of Physiology, Johns Hopkins University School of Medicine, Baltimore, MD 21205, USA
[5]National Facility for Protein Science in Shanghai, Zhangjiang Lab, Shanghai Advanced Research Institute, Chinese Academy of Science, Shanghai 201210, China
[6]Shanghai Science Research Center, Chinese Academy of Sciences, Shanghai 201204, China
[7]Institute of Neuroscience and State Key Laboratory of Neuroscience, CAS Center for Excellence in Brain Science and Intelligence Technology, Chinese Academy of Sciences, Shanghai 200031, China
[8]CAS Key Laboratory of Molecular Virology & Immunology, Institut Pasteur of Shanghai, University of Chinese Academy of Sciences, Chinese Academy of Sciences, Shanghai 200031, China
[9]Key Laboratory of Cell Proliferation and Differentiation of the Ministry of Education, School of Life Sciences, Peking University, Peking-Tsinghua Center for Life Sciences, Beijing 100871, China
[10]Affiliated Cancer Hospital & Institute of Guangzhou Medical University, State Key Laboratory of Respiratory Diseases, Guangzhou Medical University, Guangzhou, Guangdong 510180, China
[11]Department of Pathology, Case Western Reserve University School of Medicine, Cleveland, OH 44106, USA
[12]State Key Laboratory of Virology, College of Life Sciences, Wuhan University, Wuhan, Hubei 430072, China
[13]Center for Allergic and Inflammatory Diseases & Department of Otolaryngology, Head and Neck Surgery, Affiliated Eye, Ear, Nose and Throat Hospital, Fudan University, Shanghai 200031, China
[14]NeuroCure Cluster of Excellence, Charité University Medicine, D-10117 Berlin, Germany
[15]These authors contributed equally
[16]Lead Contact
*Correspondence: zhaozhu@jhmi.edu (Z.Q.), jentsch@fmp-berlin.de (T.J.J.), huixiao@ips.ac.cn (H.X.)
https://doi.org/10.1016/j.immuni.2020.03.016

## SUMMARY

The enzyme cyclic GMP-AMP synthase (cGAS) senses cytosolic DNA in infected and malignant cells and catalyzes the formation of 2′3′cGMP-AMP (cGAMP), which in turn triggers interferon (IFN) production via the STING pathway. Here, we examined the contribution of anion channels to cGAMP transfer and anti-viral defense. A candidate screen revealed that inhibition of volume-regulated anion channels (VRACs) increased propagation of the DNA virus HSV-1 but not the RNA virus VSV. Chemical blockade or genetic ablation of LRRC8A/SWELL1, a VRAC subunit, resulted in defective IFN responses to HSV-1. Biochemical and electrophysiological analyses revealed that LRRC8A/LRRC8E-containing VRACs transport cGAMP and cyclic dinucleotides across the plasma membrane. Enhancing VRAC activity by hypotonic cell swelling, cisplatin, GTPγS, or the cytokines TNF or interleukin-1 increased STING-dependent IFN response to extracellular but not intracellular cGAMP. *Lrrc8e*$^{-/-}$ mice exhibited impaired IFN responses and compromised immunity to HSV-1. Our findings suggest that cell-to-cell transmission of cGAMP via LRRC8/VRAC channels is central to effective anti-viral immunity.

## INTRODUCTION

The invasion and propagation of viruses and intracellular bacteria is frequently associated with the presence of double-stranded DNAs (dsDNAs) in the cytosol, which trigger diverse host defense mechanisms including the type I interferon (IFN) response (Chen et al., 2016b; Roers et al., 2016). The enzyme cyclic GMP-AMP synthase (cGAS) acts as a sensor of cytosolic dsDNAs in infected

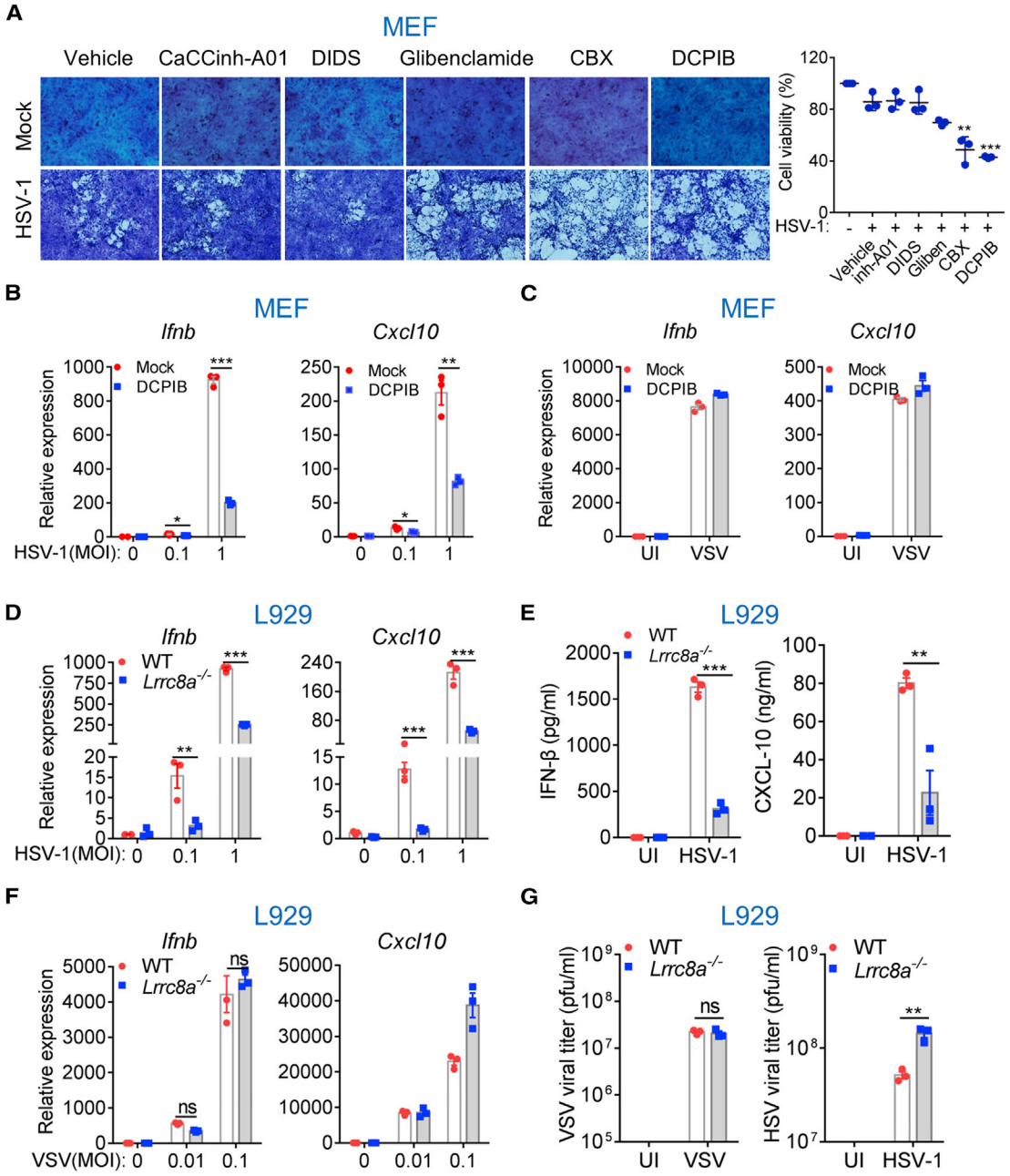


**Figure 1. VRAC Blockade Impairs HSV-Induced IFN Responses**

(A) MEFs pretreated with various chloride channel inhibitors (CaCCinh-A01 [15 μM], DIDS [60 μM], glibenclamide [30 μM], CBX [100 μM], DCPIB [20 μM]) were infected with HSV-1 (MOI: 0.01) for 36 h and then fixed and stained with 0.5% crystal violet for 2 h.

(B and C) MEFs pretreated with 20 μM DCPIB were infected with HSV-1 (MOI: 0.01) (B) or VSV (MOI: 0.01) (C) for 12 h. Real-time PCR was conducted to assess *Ifnb* and *Cxcl10* expression (n = 3 biological replicates).

(D–F) L929 cells were uninfected (UI) or infected with HSV-1 (D and E) or VSV (F) for 12 h. The IFN responses were assessed by real-time PCR (D and F) or ELISA (E) (n = 3 biological replicates).

(G) L929 cells were UI or infected with HSV-1 (MOI: 0.1) or VSV (MOI: 0.01) for 24 h. The viral titers were measured by plaque assay (n = 3 biological replicates).

Data are presented as mean ± SEM (*$p < 0.05$, **$p < 0.01$, ***$p < 0.001$; ns, not significant; analyzed by Student's t test).

See also Figure S1.

and malignant cells (Sun et al., 2013). Upon binding to dsDNA, cGAS catalyzes the formation of 2′3′cGMP-AMP (cGAMP) (Ablasser et al., 2013a; Chen et al., 2016b; Wu et al., 2013), a second messenger that directly binds to the endoplasmic reticulum (ER)-anchored adaptor protein stimulator of interferon genes (STING; also referred to as MITA or ERIS) (Ishikawa and Barber, 2008; Sun et al., 2009; Zhong et al., 2008). Subsequently, STING triggers the activation of the kinase TBK1, which then

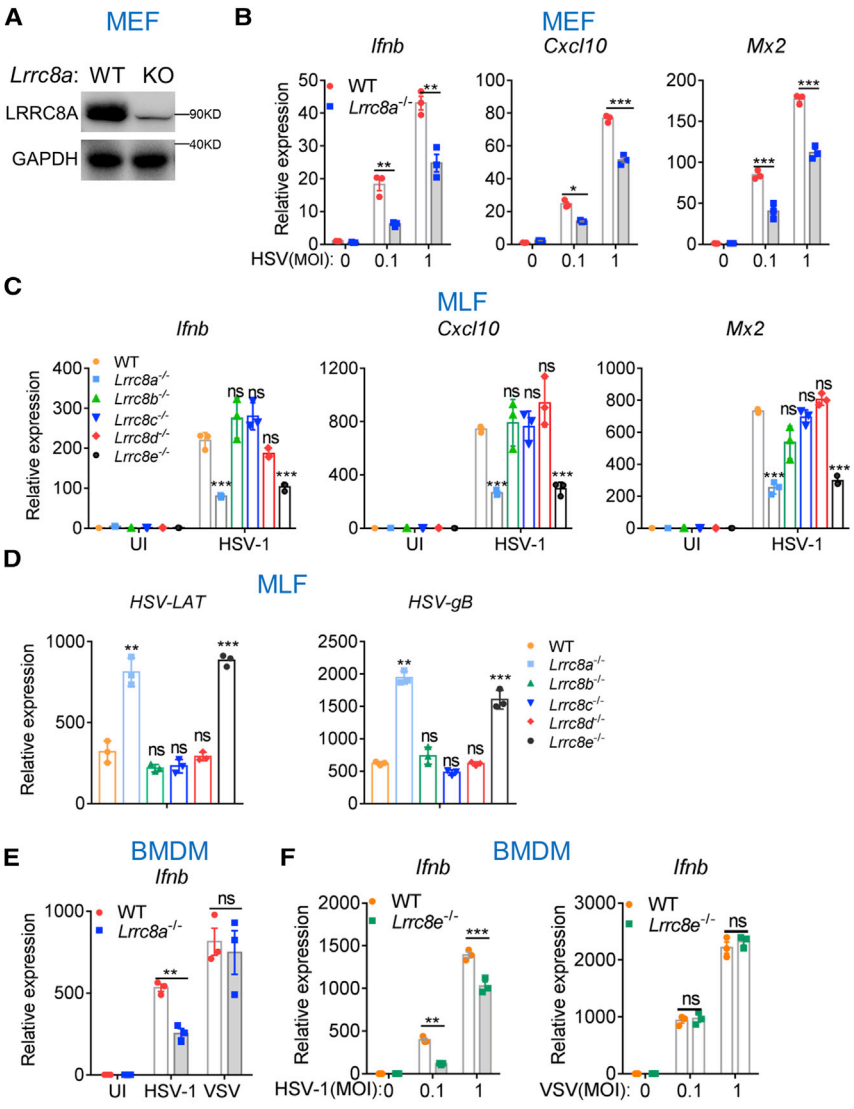


**Figure 2. LRRC8A/E-Containing VRACs Increase HSV-1-Induced IFN Responses**

(A and B) Primary WT and *Lrrc8a*$^{-/-}$ MEFs confirmed by immunoblotting (A) were infected with HSV-1 for 9 h, and the expression of *Ifnb* and *Cxcl10* were quantified by real-time PCR (B, n = 3 biological replicates).

(C and D) MLFs were uninfected or infected with HSV-1 (MOI: 0.5) for 9 h, and the expression of *Ifnb* and Isgs (C) as well as viral genes (D) were quantified by real-time PCR (n = 3 biological replicates).

(E and F) BMDMs were infected with HSV-1 or VSV (MOI: 0.1 for E, and 0.1 or 1 for F) for 9 h; the expression of *Ifnb* was quantified by real-time PCR (n = 3 biological replicates).

Data are presented as mean ± SEM (*p < 0.05, **p < 0.01, ***p < 0.001; ns, not significant; analyzed by Student's t test).

See also Figure S2.

phosphorylates the transcriptional factor IRF3 to induce a robust IFN response (Ablasser and Chen, 2019; Ablasser and Hur, 2020; Barber, 2015; Wu et al., 2013). cGAMP is uniquely produced in metazoans; however, other types of cyclic dinucleotides (CDNs) such as c-di-AMP (cdA), c-di-GMP (cdG), and 3′3′cGAMP are produced by a wide array of prokaryotes and can also activate STING to elicit IFN responses (Danilchanka and Mekalanos, 2013; Margolis et al., 2017). cGAMP produced in virus-infected cells (Ablasser et al., 2013b) or cancer cells (Chen et al., 2016a) can also be transmitted into bystander cells through gap junctions, triggering an IFN response therein. cGAMP packaged into viral particles can be transferred into newly infected cells as well (Bridgeman et al., 2015; Gentili et al., 2015). Moreover, the folate transporter Slc19a1 has been implicated in the transport of extracellular cGAMP into the cytosol of a subset of human cells (Luteijn et al., 2019; Ritchie et al., 2019).

The volume-regulated anion channel (VRAC) controls cell volume by releasing $Cl^-$ and organic osmolytes in response to cell swelling (Hoffmann et al., 2009; Jentsch, 2016; Osei-Owusu et al., 2018; Pedersen et al., 2016) and consists of a heteromer of LRRC8 proteins (Qiu et al., 2014; Voss et al., 2014). In addition to the obligatory subunit LRRC8A (also known as SWELL1), at least one of the other LRRC8 isoforms (LRRC8B, -C, -D, or -E) is needed to form hetero-multimeric channels in the plasma membrane (Voss et al., 2014). LRRC8 channels (VRACs) not only conduct $Cl^-$ and other halide ions, but also a variety of organic molecules. These include taurine (Qiu et al., 2014; Voss et al., 2014), inositol, glutamate, and other neurotransmitters (Lutter et al., 2017; Yang et al., 2019) and therapeutic agents such as cisplatin, carboplatin (Planells-Cases et al., 2015), and blasticidin S (Lee et al., 2014). Whereas all LRRC8A-containing heteromers yield swelling-activated $Cl^-$ currents, the transport of organic compounds depends on VRAC's subunit composition. Inclusion of LRRC8D enhances the transport of all tested organic substrates (Lutter et al., 2017; Planells-Cases et al., 2015), whereas inclusion of LRRC8E rather specifically stimulates the transport of the negatively charged glutamate and aspartate (Lutter et al., 2017). VRACs are thought to be important for diverse processes including insulin secretion (Best et al., 2010; Kang et al., 2018; Stuhlmann et al., 2018), neuron-glia interaction (Yang et al., 2019), stroke (Wilson et al., 2019; Yang et al., 2019), apoptosis and cancer drug resistance (Planells-Cases et al., 2015), and sperm cell development (Lück et al., 2018). The importance of VRACs is further illustrated by the multiple tissue abnormalities and lethality of *Lrrc8a*-deficient mice (Kumar et al., 2014; Platt et al., 2017). Besides activation by cell swelling, VRACs can be slowly opened by the pro-apoptotic drug cisplatin (Planells-Cases et al., 2015), GTPγS, and certain G-protein coupled receptors (Hoffmann et al., 2009; Nilius et al., 1999; Voets et al., 1998).

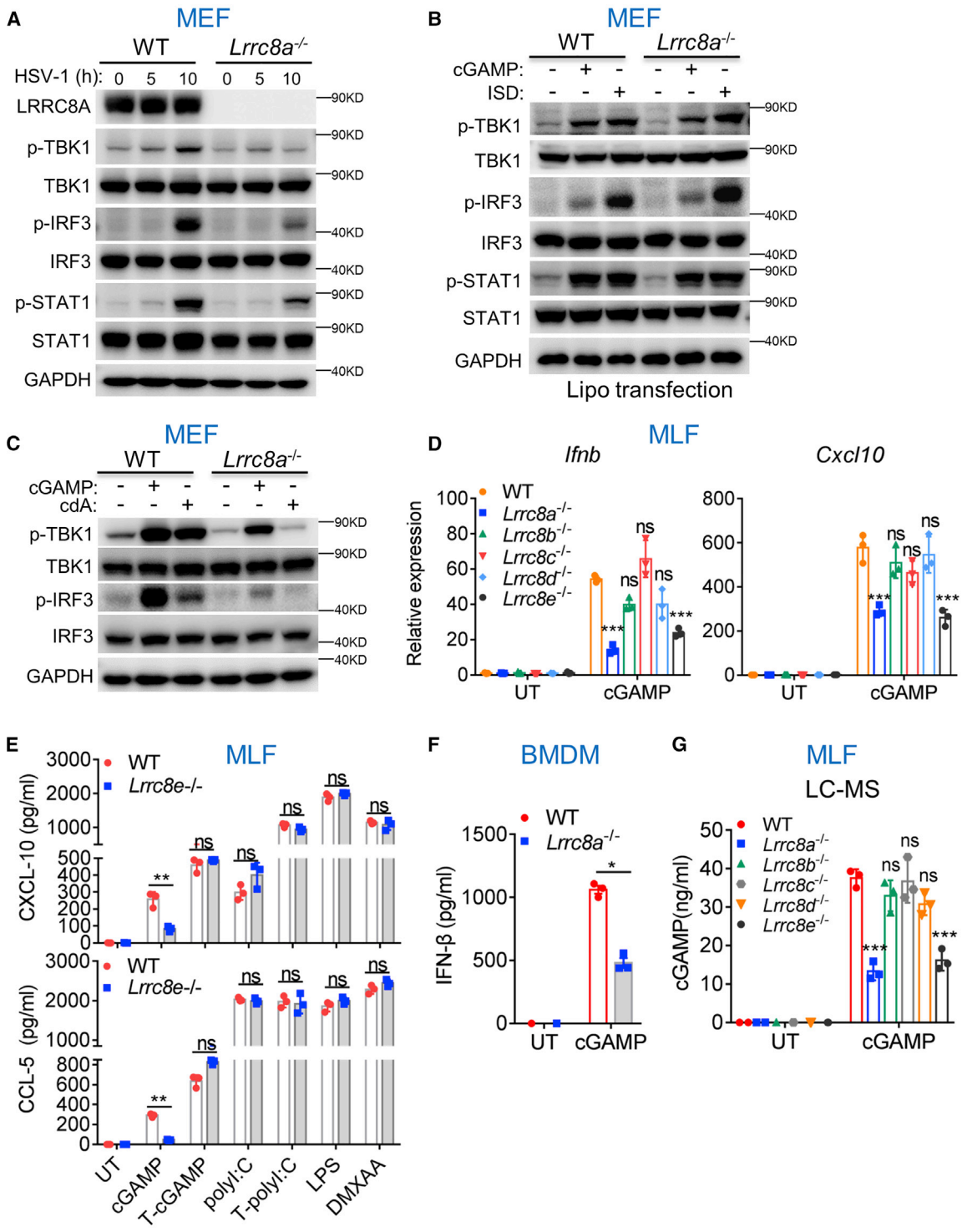


**Figure 3. LRRC8A/E-Containing VRACs Facilitate Extracellular cGAMP-, but Not Intracellular cGAMP-Induced IFN Responses**

(A–C) MEFs were treated with HSV-1 (MOI: 0.5) (A), cGAMP (2 μg/mL) or ISD (1 μg/mL) transfected with lipofectamine 2000 (B), or cGAMP (10 μg/mL) or cdA (10 μg/mL) added to media (C) for 3 h. The activation of STING signaling was assessed by immunoblotting. Data are representative of four independent experiments.

(D) MLFs were stimulated with added cGAMP (5 μg/mL) for 6 h. The expression of *Ifnb* and *Cxcl10* was quantified by real-time PCR (n = 3 biological replicates).

(E) MLFs were stimulated with cGAMP (5 μg/mL), polyI:C (10 μg/mL), LPS (100 ng/mL), DMXAA (5 μM), or lipofectamine-transfected cGAMP (2 μg/mL) or polyI:C (1 μg/mL) for 18 h. The secretion of chemokines was measured by ELISA (n = 3 biological replicates).

*(legend continued on next page)*

Here, we examined the roles of anion channels in anti-viral defense. A candidate screen revealed that inhibition of VRACs resulted in increased viral propagation upon herpes simplex virus 1 (HSV-1) infection. *Lrrc8a*$^{-/-}$ cells exhibited higher viral loads after HSV-1 infection but not vesicular stomatitis virus (VSV) infection, indicating a difference in responses to DNA versus RNA virus. The STING pathway activated by extracellular cGAMP was dampened in *Lrrc8a*$^{-/-}$ or *Lrrc8e*$^{-/-}$ cells, and further biochemical analyses revealed transport of cGAMP and CDNs across the plasma membrane by VRACs containing LRRC8A and -E. Our findings suggest that this transport is central to the host control of HSV-1 infection, likely through the induction of reinforcing IFN-β synthesis in distant bystander cells.

## RESULTS

### LRRC8 VRACs Play a Crucial Role in Anti-viral IFN Response

To explore the role of anion channels in anti-viral defense, we screened a small library of anion channel inhibitors using a cell-based viral infection platform modified from our previous study (Du et al., 2015). Infection with herpes simplex virus KOS strain (HSV-1) causes necrotic cell death in murine embryonic fibroblasts (MEFs) (Wang et al., 2014), a process often inversely correlated with IFN response. As proof of principle, *Sting*$^{-/-}$ MEFs underwent increased necrotic cell death following HSV-1 infection (Figure S1A). The screen revealed that 4-(2-Butyl-6,7-dichloro-2-cyclopentyl-indan-1-on-5-yl) oxobutyric acid (DCPIB) and carbenoxolone (CBX), two well-known VRAC inhibitors (Benfenati et al., 2009; Decher et al., 2001), augmented necrotic cell death (Figure 1A) and viral propagation (Figure S1B) following HSV-1 infection. Conversely, other anion channel blockers, including CaCCinh-A01, DIDS, and glibenclamide, lacked a notable impact on HSV-1-induced cellular pathology (Figures 1A). Interestingly, treatment with DCPIB efficiently suppressed the IFN response to the DNA virus HSV-1 (Figures 1B and S1C) but had no significant impact on the induction of *Ifnb* and *Cxcl10* by RNA virus VSV (Figure 1C). These results suggested VRAC as a potential modulator of the IFN response to DNA virus.

Given that DCPIB and CBX are non-specific VRAC inhibitors and can, for instance, also block other channels such as pannexin-1 and connexins (Ablasser et al., 2013b; Friard et al., 2017), we employed a genetic approach to validate a role of VRACs in anti-viral IFN response. Whereas RNAi of *Cx43* or *Panx1* failed to affect the HSV-1-induced IFN response, RNAi of *Lrrc8a* severely compromised the induction of *Ifnb* and *Cxcl10* (Figure S1D). To rigorously examine the role of LRRC8/VRAC channels in anti-viral defense, we disrupted the obligatory Lrrc8a subunit in L929 mouse fibroblasts by Crispr-cas9 technology. *Lrrc8a*$^{-/-}$ L929 cells exhibited blunted expression of *Ifnb* and *Cxcl10* at both mRNA (Figures 1D) and protein levels (Figure 1E). Following VSV infection, however, both wild-type (WT) and *Lrrc8a*$^{-/-}$ L929 cells elicited robust IFN response (Figure 1F) and exhibited a similar viral load (Figure 1G). Conversely, increased viral loads were associated with *Lrrc8a*-deficiency following HSV-1 infection (Figure 1G). Together, these results uncovered a role for LRRC8 VRACs in the IFN response for host defense against DNA viruses.

### LRRC8A/E-containing VRACs Promote Anti-viral IFN Response

We next sought to extend the role of LRRC8A in anti-viral response to various primary cells. First, WT and *Lrrc8a*$^{-/-}$ MEFs (Figure 2A) were created by transduction of control or Cre-expressing retroviral vector to primary MEFs isolated from *Lrrc8a*$^{f/f}$ mice (Yang et al., 2019). Upon HSV-1 infection, *Lrrc8a*$^{-/-}$ MEFs showed diminished expression of *Ifnb* and interferon stimulated genes (Isgs) *Cxcl10* and *Mx2* (Figure 2B). Moreover, *Lrrc8a*$^{-/-}$ MEFs produced less amounts of IFN-β and CXCL-10 in response to HSV-1 but not VSV infection (Figure S2A). Next, WT and *Lrrc8a*$^{-/-}$ mouse lung fibroblasts (MLFs) and bone marrow-derived macrophages (BMDMs) were generated from tamoxifen-treated *Lrrc8a*$^{f/f}$ and *Lrrc8a*$^{f/f:creERT}$ mice, respectively. Upon HSV-1 infection, *Lrrc8a*$^{-/-}$ MLFs showed markedly reduced IFN responses (Figures 2C and S2B), which were correlated with increased expression of the HSV-1 encoded genes LAT and gB (Figure 2D). Likewise, *Lrrc8a*$^{-/-}$ BMDMs showed impaired *Ifnb* responses to HSV-1 but not to VSV infection (Figures 2E and S2C). Hence, Lrrc8a participates in the anti-HSV defense in a wide range of cell types, including immune and non-immune cells.

Next, we generated mice deficient in each other subunit (*Lrrc8b*, *Lrrc8c*, *Lrrc8d*, and *Lrrc8e*) to identify which one is needed, together with Lrrc8a, for anti-viral IFN response. *Lrrc8e*-deficiency markedly reduced HSV-1-triggered IFN response, whereas deleting *Lrrc8b*, *Lrrc8c*, or *Lrrc8d* lacked a significant impact (Figure 2C). Further, MLFs deficient in *Lrrc8e*, but not *Lrrc8b–d*, showed heightened viral replication upon HSV-1 infection (Figure 2D). Furthermore, in BMDMs, *Lrrc8e*-deficiency compromised HSV-1-induced IFN response, particularly at lower MOI of viral infection (Figures 2F and S2D). Like *Lrrc8a*$^{-/-}$ BMDMs (Figure 2E), *Lrrc8e*$^{-/-}$ BMDMs displayed a normal IFN response to VSV infection (Figures 2F and S2D). Genetic deletion or RNAi of *Lrrc8e* in L929 cells also severely disrupted IFN responses to HSV-1 infection (Figures S2E and S2F). Hence, incorporation of the Lrrc8e subunit into Lrrc8a-containing heteromeric VRACs is crucial for their role in anti-viral IFN response.

### LRRC8A/E-containing VRACs Enhance Extracellular cGAMP-induced STING Activation

To understand how LRRC8A/E-containing VRACs regulate anti-viral IFN responses, we examined the corresponding signaling in WT and VRAC-deficient cells. In WT MEFs, both HSV-1 and VSV infection robustly activated TBK1 and IRF3 as evident from markedly increased phosphorylation, and also STAT1 whose phosphorylation is dependent on a feedback response by autocrine or paracrine IFN (Figures 3A and S3A). *Lrrc8a* ablation

(F) BMDMs were treated with cGAMP (5 μg/mL) for 12 h, and the secreted IFN-β was measured by ELISA (n = 3 biological replicates).
(G) MLFs were treated with cGAMP (2 μg/mL) for 1 h, and the cytosolic cGAMP was quantified by LC-MS (n = 3 biological replicates).
Data are presented as mean ± SEM (*p < 0.05, **p < 0.01, ***p < 0.001; ns, not significant; analyzed by Student's t test). UT, untreated.
See also Figure S3.

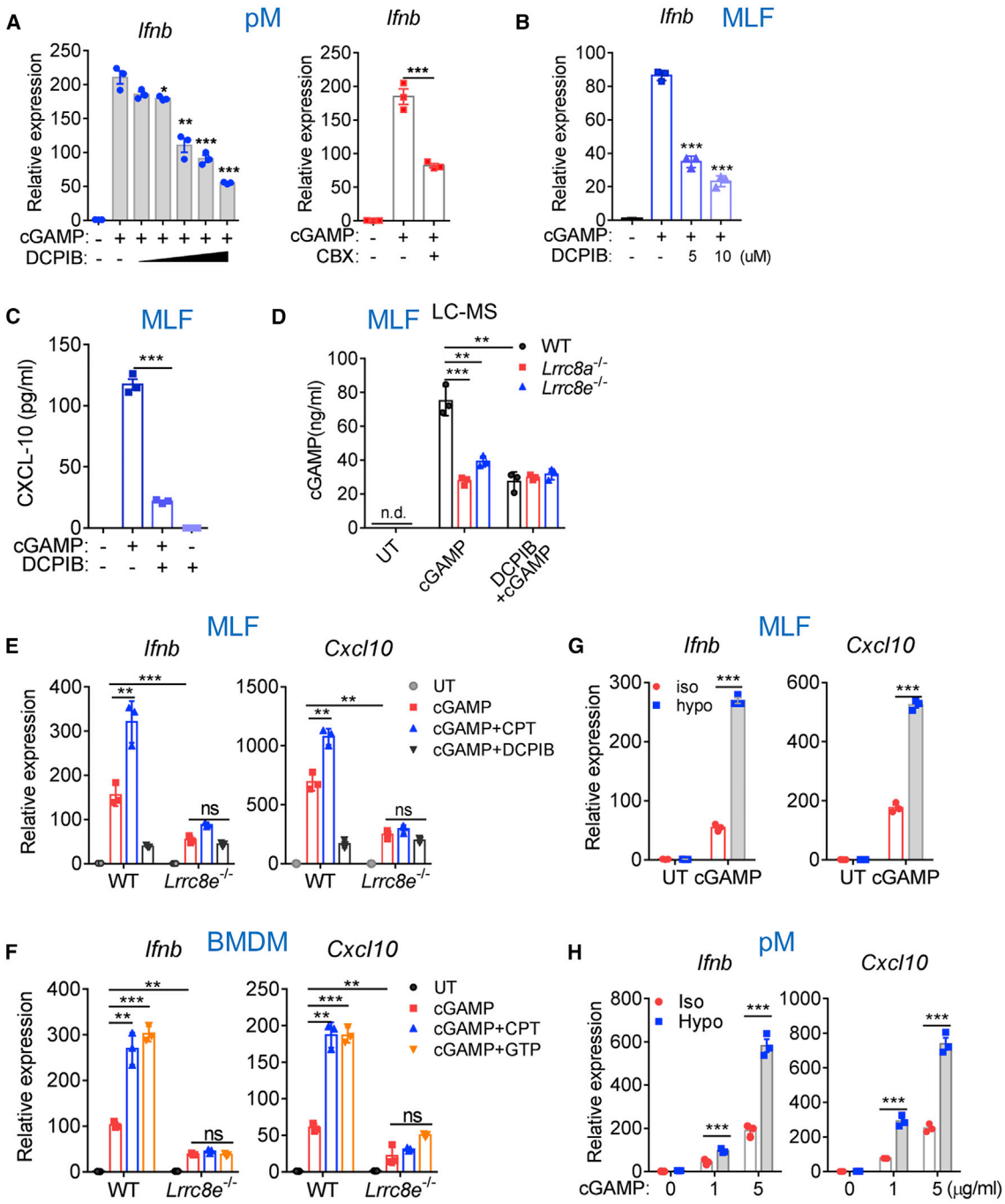


**Figure 4. VRAC Channel Activity Positively Correlates with Extracellular cGAMP Responses**

(A) pMs were stimulated with 5 μg/mL cGAMP for 3 h in the presence of various amounts (5–80 μM) of DCPIB or 100 μM CBX. The expression of *Ifnb* was measured by real-time PCR (n = 3 biological replicates).

(B and C) MLFs were stimulated with 5 μg/mL cGAMP for 6 h with or without 5–10 (B) or 10 (C) μM DCPIB. The expression of *Ifnb* and *Cxcl10* was measured by real-time PCR (B) or ELISA (C) (n = 3 biological replicates).

(D) MLFs were treated with cGAMP (5 μg/mL) for 1 h with or without 10 μM DCPIB. The cytosolic cGAMP was quantified by LC-MS (n = 3 biological replicates).

(E) MLFs were treated with 5 μg/mL cGAMP for 6 h in the presence of 50 μM cisplatin (CPT) or 20 μM DCPIB. The expression of *Ifnb* and *Cxcl10* was measured by real-time PCR (n = 3 biological replicates).

(F) BMDMs were stimulated with 5 μg/mL cGAMP in the presence of 50 μM CPT or 300 μM GTPγS for 6 h. The expression of *Ifnb* and *Cxcl10* was measured by real-time PCR (n = 3 biological replicates).

(G) MLFs under isotonic or hypotonic conditions were stimulated with 5 μg/mL cGAMP for 3 h. The induction of *Ifnb* and *Cxcl10* was analyzed by real-time PCR (n = 3 biological replicates).

*(legend continued on next page)*

reduced the phosphorylation of TBK1, IRF3, and STAT1 upon infection with HSV-1 but not VSV in MEFs (Figures 3A and S3A). Because HSV-1 primarily engages the cGAS/STING pathway, whereas VSV predominantly acts through RIG-I/MAVS, we reasoned that LRRC8/VRAC channels might impinge on cGAS/STING signaling. However, directly activating cGAS by transfection of interferon stimulating DNA (ISD) triggered similar TBK1 and IRF3 activation in WT and *Lrrc8a*$^{-/-}$ (Figure 3B) or *Lrrc8e*$^{-/-}$ MEFs (Figure S3B). Likewise, transfecting cGAMP into the cytosol to directly activate STING resulted in similar phosphorylation of TBK1, IRF3, and STAT1 in WT and *Lrrc8a*$^{-/-}$ cells (Figure 3B). Hence, whereas VRACs are important for activating STING-dependent signaling upon HSV-1 infection, they do not influence the signaling events elicited by cytosolic agonists of cGAS or STING. Similar cGAMP production in WT and *Lrrc8a*$^{-/-}$ cells upon HSV-1 infection (Figure S3C) excluded a role for VRACs in cGAMP synthesis.

Given VRACs' ability to transport metabolites and drugs, we wondered whether VRACs may transport cGAMP from infected cells to bystander cells where it may elicit an additional IFN response through STING. To indirectly measure cGAMP uptake though VRACs, we added cGAMP to culture media without transfection reagent and measured the induced IFN responses. Despite being hydrophilic and hence poorly permeable through lipid bilayers, extracellular cGAMP triggered marked phosphorylation of TBK1 and IRF3 in WT MEFs (Figure 3C). Similar effects were observed with extracellularly added bacterial cdA and 3′3′cGAMP (Figures 3C and S3D). Importantly, added cGAMPs and cdA induced much less phosphorylation on TBK1 and IRF3 in *Lrrc8a*$^{-/-}$ MEFs (Figures 3C and S3D). Also, with MLFs, added cGAMP strongly induced *Ifnb* and *Cxcl10* expression in WT, but much less in *Lrrc8a*$^{-/-}$ cells (Figure 3D). Mirroring the roles of Lrrc8a and Lrrc8e in response to HSV-1 infection, ablation of *Lrrc8e* but not of *Lrrc8b*, *-c*, or *-d* significantly reduced the IFN response to cGAMP extracellularly added to MLFs (Figure 3D). *Lrrc8e*-deficiency also impaired the secretion of CXCL-10 and CCL-5 in response to extracellular but not to transfected cGAMP or to the cell permeable STING agonist DMXAA, LPS, or polyI:C (Figure 3E). Consistently, extracellular cGAMP induced less IFN-β production in *Lrrc8a*$^{-/-}$ BMDMs (Figure 3F) or MLFs (Figure S3E). These results indicate that Lrrc8a/e-containing VRACs may have a role in transporting cGAMP through the plasma membrane.

The notion that Lrrc8e-containing VRACs mediate cGAMP transport was further buttressed by direct measurements of cellular cGAMP uptake using liquid chromatography-mass spectrometry (LC-MS) (Figure 3G). Ablation of either *Lrrc8a* or *Lrrc8e* but not of *Lrrc8b-d* decreased uptake of cGAMP into the cytosol by roughly 60% (Figure 3G). Collectively, these data strongly suggest that Lrrc8e-containing VRACs may operate as a cell membrane conduit for cGAMP entry. With its larger size, extracellularly added FITC-conjugated cGAMP was unable to trigger *Ifnb* and *Cxcl10* expression (Figure S3F) or induce IRF3 phosphorylation (Figure S3G), although it elicited robust TBK1/IRF3 phosphorylation when transfected with liposomes (Figure S3H).

## The Response to Extracellular cGAMP Depends on VRAC Channel Activity

If cGAMP permeates through VRAC's ion conducting pore, the cellular effects of externally added cGAMP are expected to be similarly affected by procedures that block or enhance VRAC-mediated $Cl^-$ currents. Indeed, VRAC blockade with DCPIB or CBX diminished extracellular cGAMP-induced *Ifnb* and *Cxcl10* expression in peritoneal macrophages (pMs) (Figure 4A) and MLFs (Figures 4B and 4C). Whereas DCPIB inhibited the uptake of extracellular cGAMP in WT cells by roughly 60%, it did not affect uptake into *Lrrc8a*$^{-/-}$ or *Lrrc8e*$^{-/-}$ cells (Figure 4D). Conversely, DCPIB lacked significant impact on IFN responses to LPS, polyI:C, or IFN-β (Figures S4A–S4C). Hence, cellular effects of extracellular cGAMP are impaired when VRAC's ion-conducting pore is blocked.

By contrast, GTPγS and cisplatin, two agents capable of potentiating VRAC activity (Planells-Cases et al., 2015; Voets et al., 1998), markedly enhanced extracellular cGAMP-induced IFN response in MLFs, BMDMs, and L929 cells (Figures 4E, 4F, and S4D). As expected, GTPγS- or cisplatin-enhanced cGAMP response was abrogated in *Lrrc8a*$^{-/-}$ or *Lrrc8e*$^{-/-}$ cells (Figures 4E, 4F, and S4D). Strikingly, hypotonic cell swelling, the most potent stimulus for opening VRACs, greatly enhanced cGAMP-induced IFN responses in various mouse primary cells (MLF, pM, and MEF) (Figures 4G, 4H, and S4E) and human cells (HeLa and THP-1) (Figures S4F and S4G). Collectively, these data strongly support the notion that cGAMP permeates VRAC's pore.

## Hypotonic Activation of VRACs Enhances the Entry of Extracellular cGAMP

Although cell swelling robustly enhanced the IFN response to extracellular cGAMP, it failed to augment responses to intracellularly delivered cGAMP (Figure S5A). It neither potentiated LPS-, polyI:C-, or IFN-β-induced gene expression (Figures S5B and S5C). Cell swelling-promoted IFN responses to extracellular cGAMP were markedly reduced in *Lrrc8a*$^{-/-}$ L929 and MEFs (Figures 5A, 5B, and S4E), and in L929 or BMDM lacking *Lrrc8e* (Figures 5A and 5C). In contrast, Lrrc8b, -c, and -d apparently lacked a significant role in cell swelling-promoted cGAMP response (Figure S5D). Likewise, RNAi of *Panx1* or *Cx43* did not affect the response to extracellular cGAMP in the setting of cell swelling (Figure S5E).

In contrast to hypotonic swelling, exposure to hypertonic medium did not influence extracellular cGAMP-induced IFN response (Figure S5F). Hypotonicity-boosted *Ifnb* expression was abrogated by DCPIB but not by glibenclamide or CaCCinh-A01, excluding the involvement of several other $Cl^-$ channels (Figure 5D). Cellular depletion of $Cl^-$ did not abolish the effect of hypotonicity on the extracellular cGAMP response, suggesting $Cl^-$ efflux is not required for cGAMP transport

(H) pMs under isotonic or hypotonic conditions were stimulated with cGAMP (1 or 5 μg/mL) for 3 h. The induction of IFN response was measured by real-time PCR (n = 3 biological replicates).

Data are presented as mean ± SEM and analyzed by Student's t test (*p < 0.05, **p < 0.01, ***p < 0.001). UT, untreated; n.d., not detected.

See also Figure S4.

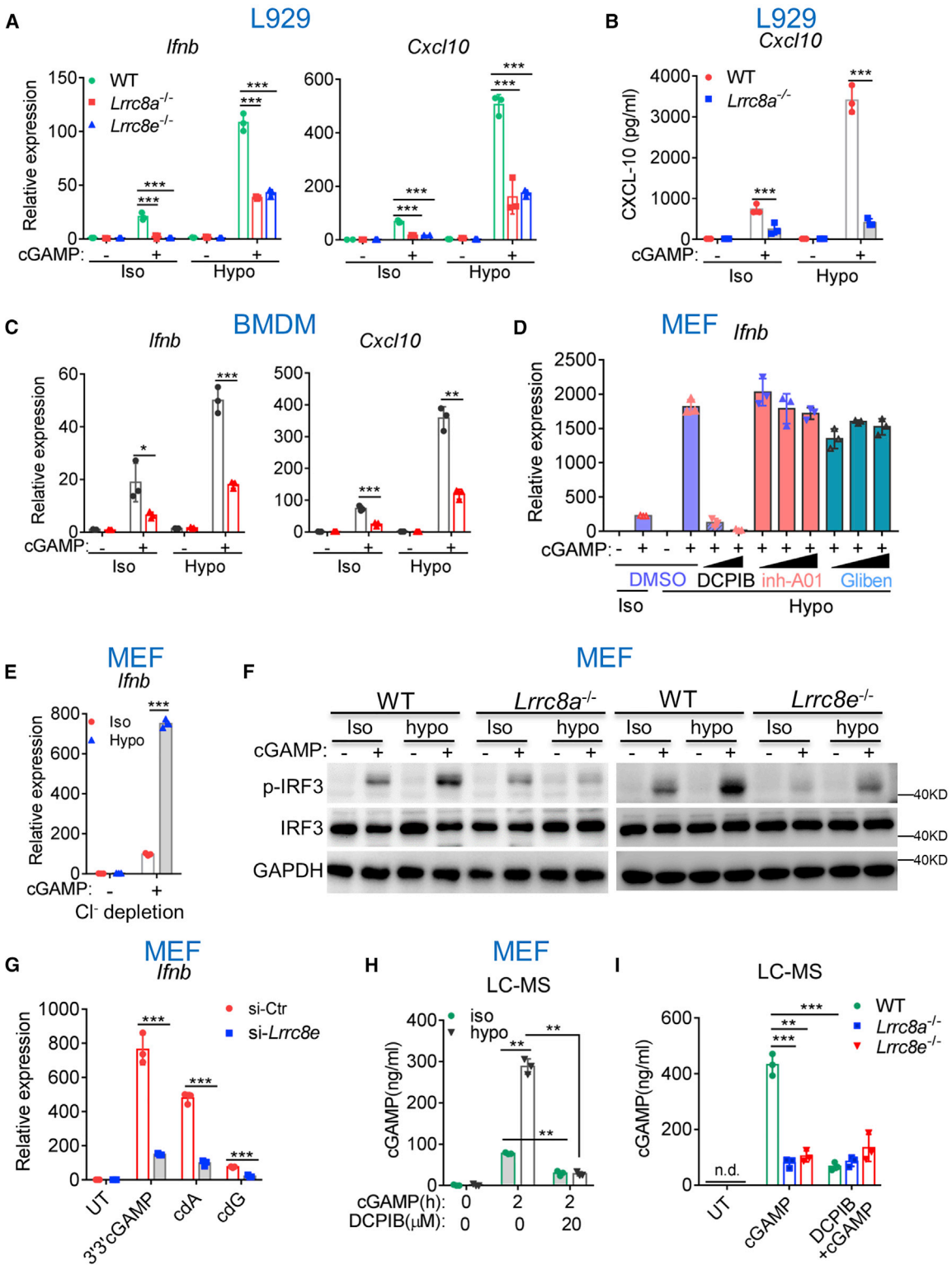


**Figure 5. Hypotonic Swelling Enhances VRAC Transport of cGAMP and CDNs**

(A) L929 cells were stimulated with 5 μg/mL cGAMP for 3 h under isotonic or hypotonic conditions. The induction of *Ifnb* and *Cxcl10* was analyzed by real-time PCR (n = 3 biological replicates).

(B) L929 cells stimulated with 5 μg/mL cGAMP for 3 h under isotonic or hypotonic conditions were then cultured with normal media for another 12 h. The secretion of CXCL-10 was measured by ELISA (n = 3 biological replicates).

*(legend continued on next page)*

(Figure 5E). Cell swelling augmented extracellular cGAMP-elicited IRF3 phosphorylation, which was contingent on the expression of Lrrc8a or Lrrc8e in various cell types including MEF (Figure 5F), BMDM (Figure S5G), L929 (Figure S5H), and HeLa (Figure S5I).

Under hypotonic condition, bacterial cdA, cdG, and 3′3′cGAMP also induced robust IFN responses, which were severely diminished in *Lrrc8e*-RNAi cells (Figure 5G). Finally, we measured cGAMP entry by LC-MS in response to osmotic cell swelling. Hypotonicity profoundly enhanced cGAMP entry into cells (Figure 5H), a process that was strongly inhibited by DCPIB (Figure 5H) or genetic ablation of *Lrrc8a* or *Lrrc8e* (Figure 5I). Together, these data support a central role for Lrrc8e-containing VRACs in transporting cGAMPs and CDNs.

## LRRC8A/E-containing VRACs Transmit cGAMP to Bystander Cells

Upon HSV-1 infection, cGAMP was detected in MEFs (Figure 6A), which were all viable (Figure S6A), and in the surrounding medium (Figure 6B), as quantified by LC-MS and more sensitive ELISA (Gentili et al., 2019), respectively. Heat-inactivated media from HSV-1-infected WT MEFs induced *Ifnb* expression in WT but not *Lrrc8a*$^{-/-}$ recipient cells in a STING-dependent but cGAS-independent manner (Figure 6C). Preincubation with snake venom phosphodiesterase I (SVPDE), a cGAMP hydrolase (Ablasser et al., 2013b), abrogated the ability of culture media from HSV-1-infected cells to induce IFN response (Figure S6B). Media collected from HSV-1-infected *Lrrc8a*$^{-/-}$ cells showed less cGAMP (Figure 6B) or reduced capacity to trigger *Ifnb* than those from HSV-1-infected WT cells (Figure S6C), although their intracellular cGAMP productions were comparable (Figure S3C). Hence, VRAC probably mediates not only the uptake but also the export of cGAMP.

In addition to HSV-1, adenovirus (Lam et al., 2014) and murine cytomegalovirus (MCMV) (Bridgeman et al., 2015; Stempel et al., 2019) also engage the cGAS/STING pathway to mount IFN responses. Both adenovirus and MCMV propagated more efficiently in *Lrrc8a*$^{-/-}$ MEFs than WT controls (Figure 6D), suggesting a more general role for VRACs in the host defense against DNA viruses. We then tested whether cGAMP produced by DNA virus-infected cells could activate STING in bystander cells, using the formation of perinuclear STING aggregates as readout for STING activation by cGAMP (Ishikawa et al., 2009; Luo et al., 2016) (Figure S6D). We used adenovirus-GFP to infect WT or *Lrrc8a*$^{-/-}$ MEFs that were transiently transfected with a STING-cherry plasmid. After low MOI infection, cells infected with adenovirus-GFP exhibited prominent green fluorescence and STING-cherry aggregates (Figure 6E). STING-cherry aggregates were also detected in uninfected cells identified by the absence of green fluorescence. These cells were often physically separated from infected cells (Figure 6E). In *Lrrc8a*$^{-/-}$ MEFs, STING aggregates were much less prominent in distant uninfected cells (Figure 6E).

To further test whether cGAMP can be transmitted through VRACs from infected cells to bystander cells, we co-cultured HSV-1 pre-infected cells with uninfected bystander WT or *Lrrc8a*$^{-/-}$ MEFs separated by a transwell filter for 6 h. We then measured the IFN response in the bystander cells. Remarkably, while physically separated, bystander WT but not *Lrrc8a*$^{-/-}$ cells showed IFN induction (Figure 6F). Although bystander IFN response was abolished in *Sting*$^{-/-}$ cells, a considerable induction of *Ifnb* was detected in *Cgas*$^{-/-}$ cells (Figure S6E). The moderate reduction in IFN response observed in *Cgas*$^{-/-}$ bystander cells (Figures 6C and S6E) might be attributable to an unexpected role of cGAS in the extracellular cGAMP response (Liu et al., 2019). Importantly, inclusion of DCPIB (Figure S6E) during the co-culture diminished IFN response in WT but not *Lrrc8a*$^{-/-}$ recipients. Unlike HSV-1-infected cells, VSV-infected cells did not trigger significant *Ifnb* expression in transwell-separated bystander cells (Figure S6F). We also investigated the transmission of cGAMP from donor cells in which cGAMP synthesis was not stimulated by infection but rather by transfection with DNA or overexpression of cGAS. These cells also induced marked Lrrc8a- and STING-dependent IFN induction in bystander cells (Figure 6G). Hence, cGAMP can be transmitted to bystander cells to elicit a reinforcing IFN response.

To test whether cGAMP can directly pass through VRAC channel pores, we performed whole-cell patch-clamp recordings. Intracellular $Cl^-$ was replaced with an equal concentration of $cGAMP^{2-}$ as the only permeant anion, and VRACs were activated by perfusion of hypotonic bath solution. The negatively charged cGAMP carried small but notable inward currents representing $cGAMP^{2-}$ efflux from WT HeLa (Figure 6H) and HCT116 (Figure S6G) cells. The leftward shifts in reversal potential indicated that the cGAMP permeability of VRAC is significant,

(C) BMDMs in isotonic or hypotonic buffer were stimulated with 5 μg/mL cGAMP for 3 h. The induction of *Ifnb* and *Cxcl10* was analyzed by real-time PCR (n = 3 biological replicates). Gray bar: WT; red bar: *Lrrc8e*$^{-/-}$.

(D) MEFs were stimulated with 5 μg/mL cGAMP under isotonic or hypotonic conditions in the presence of various inhibitors (10–20 μM DCPIB; 2–10 μM CaCCinh-A01; 10–40 μM glibenclamide). The induction of *Ifnb* expression was quantified by real-time PCR (n = 3 biological replicates).

(E) MEFs were pretreated with low chloride isotonic buffer for 12 h, and then stimulated with 5 μg/mL cGAMP in low chloride isotonic or hypotonic buffer. The expression of *Ifnb* was quantified by real-time PCR (n = 3 biological replicates).

(F) MEFs were stimulated with 5 μg/mL cGAMP for 3 h under isotonic or hypotonic conditions. The signaling events were examined by immunoblotting. Data are representative of three independent experiments.

(G) MEFs were stimulated with 5 μg/mL 3′3′cGAMP, or 10 μg/mL cdA or cdG for 3 h under hypotonic condition. The induction of *Ifnb* was analyzed by real-time PCR (n = 3 biological replicates).

(H) MEFs were treated with 5 μg/mL cGAMP for 1 h under isotonic or hypotonic condition, and the cytosolic cGAMP was quantified by LC-MS (n = 3 biological replicates).

(I) MEFs were treated with 5 μg/mL cGAMP for 1 h under hypotonic condition with or without 10 μM DCPIB. The cytosolic cGAMP was quantified by LC-MS (n = 3 biological replicates).

Data are presented as mean ± SEM (*p < 0.05, **p < 0.01, ***p < 0.001; by Student's t test). UT, untreated; n.d., not detected.

See also Figure S5.

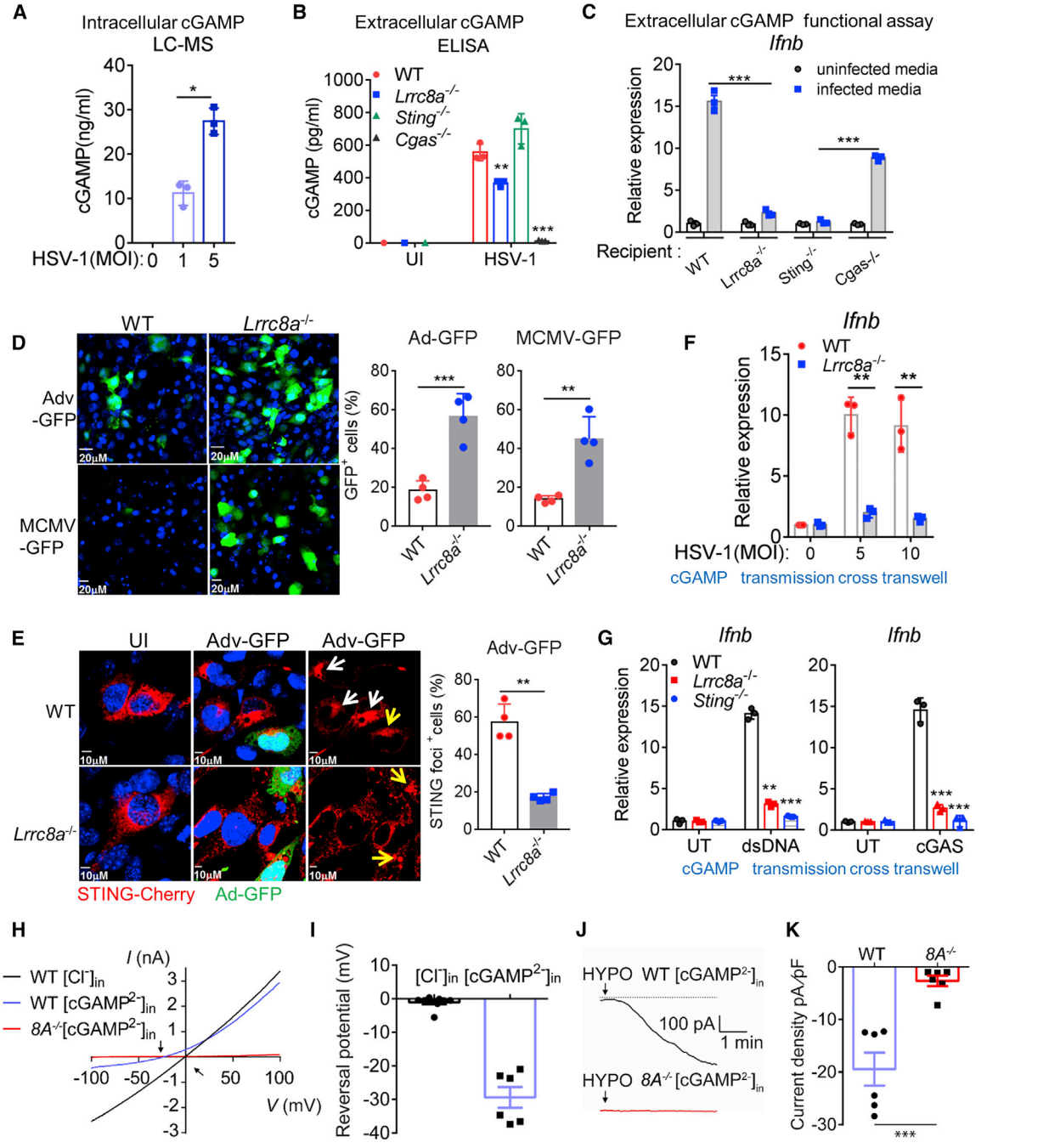


**Figure 6. LRRC8 VRACs Directly Transport cGAMP to Bystander Cells**

(A and B) MEFs were infected with HSV-1 (MOI: 1–5 for A and 5 for B) for 3 h. The cytosolic cGAMP was quantified by LC-MS (A), and the extracellular cGAMP was quantified by ELISA (B) (n = 3 biological replicates).

(C) The supernatants from MEFs uninfected or infected with HSV-1 (MOI: 5) for 3 h were then incubated with uninfected recipient WT, *Lrrc8a*$^{-/-}$, *Sting*$^{-/-}$, or *Cgas*$^{-/-}$ MEFs for another 3 h. The induction of *Ifnβ* in the recipient MEFs was analyzed by real-time PCR (n = 3 biological replicates).

(D) WT and *Lrrc8a*$^{-/-}$ MEFs were infected with adenovirus-GFP (MOI: 0.01) or MCMV-GFP (MOI: 0.01) for 24 h, and the GFP-positive cells were visualized by a fluorescence confocal microscope and quantified by ImageJ (n = 4 biological replicates).

(E) WT and *Lrrc8a*$^{-/-}$ MEFs transfected with STING-Cherry expressing plasmids for 12 h were then infected with adenovirus-GFP (MOI: 0.01) for another 12 h (n = 4 biological replicates). White arrows indicate STING aggregates in the uninfected cells, and yellow arrows indicate STING aggregates in the infected cells.

(F) *Sting*$^{-/-}$ MEFs seeded on transwell chambers were infected with HSV-1 (MOI: 5) for 3 h, and then co-cultured with WT or *Lrrc8a*$^{-/-}$ MEFs plated on six-well plates for 6 h. The induction of *Ifnβ* and *Mx2* in the recipient cells was analyzed by real-time PCR (n = 3 biological replicates).

(G) Transwell seeded *Sting*$^{-/-}$ MEF cells and HEK293 cells were transfected with dsDNA for 3 h or a plasmid expressing cGAS for 12 h, respectively, then co-cultured with various genotypes of recipient MEFs for 9 h. The induction of *Ifnβ* in the recipient cells was analyzed by real-time PCR (n = 3 biological replicates).

*(legend continued on next page)*

although less than that of $Cl^-$ (estimated $P_{cGAMP}/P_{Cl}$: ~0.1 assuming all intracellular cGAMP as free divalent anions) (Figure 6I). The cGAMP-mediated inward currents were abolished in *LRRC8A*$^{-/-}$ HeLa cells (Figures 6H, 6J, and 6K) and were blocked by DCPIB (Figure S6G). Notably, the VRAC $Cl^-$ currents were not blocked by extracellular 200 μM cGAMP (Figure S6H). These data strongly support VRAC as a direct conduit for cGAMP.

### LRRC8A/E-containing VRACs Facilitate the Host Defense against HSV-1

Contrasting with severely affected *Lrrc8a*$^{-/-}$ mice (Kumar et al., 2014), *Lrrc8e*$^{-/-}$ mice were viable and lacked an obvious phenotype. We intravenously infected *Lrrc8e*$^{-/-}$ mice and their control littermates with HSV-1. WT mice rapidly launched a robust IFN response, secreting large amounts of IFN-β, CXCL-10, CCL-5, and TNF into the bloodstream 24 h post-infection (Figure 7A). In contrast, *Lrrc8e*$^{-/-}$ mice had severely compromised response to HSV-1 infection, showing marked reduction in IFN-β, CXCL-10, CCL-5, and TNF (Figure 7A). Moreover, compared to WT mice, expression levels of *Ifnb*, *Cxcl10*, and *Ccl5* were considerably lower in the lung and liver tissues of *Lrrc8e*$^{-/-}$ mice (Figure 7B). Viral gene expression was increased in multiple tissues of *Lrrc8e*$^{-/-}$ mice (Figure 7C), correlating with heightened viral loads in the liver and kidney of *Lrrc8e*$^{-/-}$ mice (Figure 7D). Consequently, *Lrrc8e*$^{-/-}$ mice displayed much more severe morbidity and greater weight loss than WT mice throughout the course of infection (Figure 7E). Notably, following VSV infection for 24 h, both WT and *Lrrc8e*$^{-/-}$ mice produced similar amounts of IFN-β, CXCL-10, and TNF in their sera (Figure S7A). We conclude that Lrrc8e-containing VRACs play a crucial role in host defense against DNA virus HSV-1 *in vivo*.

Considering a crucial role for VRAC in anti-viral IFN response, we wondered whether VRAC-mediated cGAMP transmission could be enhanced by inflammation. We screened cytokines and growth factors for their ability to influence the IFN response to extracellular cGAMP. The cytokine TNF enhanced extracellular cGAMP-induced *Ifnb* expression in BMDMs (Figure S7B). Notably, TNF by itself neither raised intracellular cGAMP-induced *Ifnb* expression nor exerted a notable effect in *Lrrc8a*$^{-/-}$ BMDMs (Figure S7C). While being ineffective in BMDMs, IL-1β markedly increased extracellular cGAMP-induced response in MEFs, as did TNF (Figure S7D). IL-1β's effect likewise depended on the extracellular presence of cGAMP and functional VRAC channels (Figures S7D and S7E). Measurement of cGAMP uptake confirmed that TNF and IL-1β enhanced cGAMP transport through VRACs (Figure S7F), suggesting VRACs as both an effector and a propagator of inflammation.

## DISCUSSION

Here, we found that volume-regulated LRRC8/VRAC channels were critically involved in the host defense against DNA viral infection by transporting cGAMP across the plasma membrane. Promotion of cGAMP-STING-dependent IFN responses in distant bystander cells may provide support to the infected cells. Our findings also suggest that cGAMP transmission through VRACs can be boosted by a diversity of stimuli including cell swelling, anti-cancer drugs, and cytokines.

The cGAS-STING pathway has the capacity to launch robust IFN responses, but highly pathogenic viruses often dampen or cripple this pathway. For example, HSV-encoded ICP27 can interfere with TBK1 activation and thereby prevent virus-infected cells from producing IFN response (Christensen et al., 2016). The host must evolve effective countermeasures, and bystander immune activation has emerged as an effective mechanism for thwarting viral immune evasion (Holmgren et al., 2017). cGAMP can be transported to neighboring cells via gap-junctions (Ablasser et al., 2013b) or Slc19a1 (Luteijn et al., 2019; Ritchie et al., 2019). We discovered a role for VRACs as a conduit for transporting cGAMP into bystander cells in which it reinforces the STING-dependent IFN response. Whereas gap-junctions only allow cGAMP transmission between physically connected cells, VRACs may facilitate the transfer of cGAMP into distant bystander cells, thereby reaching a larger number of cells. Only a subset of human cells exhibits Slc19a1-dependent cGAMP uptake, which was not seen in several mouse cell types tested (Luteijn et al., 2019). Likewise, we found that different cell types from both human and mouse exhibited variable VRAC-mediated cGAMP transport. Notably, although Lrrc8e-containing VRACs did not directly affect cGAMP production or cGAMP-triggered STING activation in virus-infected cells, ablation of *Lrrc8e* in mice resulted in compromised IFN response and ineffective defense against HSV-1 infection, thus supporting the notion that cGAMP transmission to the bystander cells is an effective countermeasure to DNA viral infection. Ablation of *Lrrc8a*, which totally abolishes VRAC activity, inhibited cGAMP uptake by only ~50%–70% in a wide range of cell lines and primary cells. The remainder may reflect the transport activity of the plasma membrane folate transporter Slc19a1 (Luteijn et al., 2019; Ritchie et al., 2019), P2X7 purinergic receptors (Zhou et al., 2020), or yet to be identified transporters (Liu et al., 2019). LRRC8 VRACs may work in concert with these transporters to conduct cGAMP and CDNs in a cell type- and context-dependent manner.

LRRC8 VRACs are largely but probably not completely closed under resting conditions. Indeed, VRAC-mediated transport of cisplatin (Planells-Cases et al., 2015) or glutamate (Yang et al., 2019) can occur without opening VRAC with hypotonic swelling or other stimuli. We found that VRACs transported cGAMP also

(H) Hypotonicity (HYPO)-activated whole-cell currents from WT and *LRRC8A*$^{-/-}$ HeLa cells with $Cl^-$-based (50 mM NaCl) or $cGAMP^{2-}$-based (50 mM $Na_2$cGAMP) intracellular pipette solution. Arrows indicate the reversal potentials.

(I) Quantification of the reversal potentials of HYPO-activated VRAC currents in WT HeLa cells, n = 9 cells for $Cl^-$-based recording, n = 6 cells for $cGAMP^{2-}$ based recording.

(J) Time-course of HYPO-activated whole-cell currents at −100 mV for WT and *LRRC8A*$^{-/-}$ HeLa cells with $cGAMP^{2-}$-based pipette solution.

(K) Quantification of baseline subtracted HYPO-activated current densities at −100 mV in WT and *LRRC8A*$^{-/-}$ HeLa cells with $cGAMP^{2-}$ based pipette solution. n = 6 for each group.

Data are presented as mean ± SEM and analyzed by Student's t tests, *p < 0.05, **p < 0.01, ***p < 0.001. UT, untreated; UI, uninfected.

See also Figure S6.

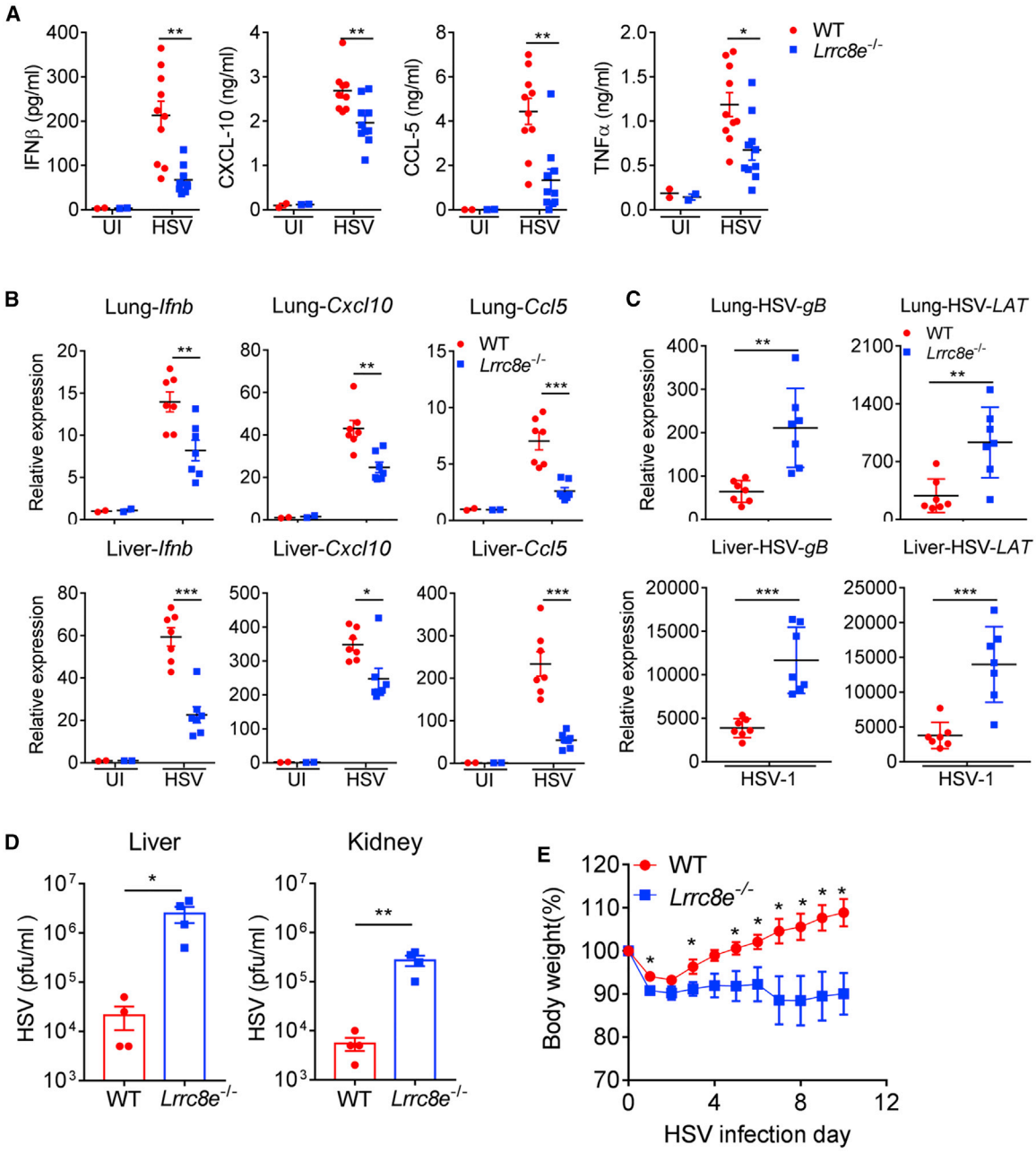


**Figure 7. LRRC8A/E-Containing VRACs Promote Host Defense to HSV-1**

8-week-old WT and *Lrrc8e*$^{-/-}$ C57BL/6N littermates including both sexes were intravenously infected with HSV-1 (1 × $10^7$ pfu/mouse).

(A–C) The sera and tissues were collected in 24 h for ELISA (A) (n = 10 mice) or real-time PCR assay of IFN response (B) or viral gene expression (C) (n = 7 mice), respectively.

(D) Plaque assay on tissues from HSV-1-infected mice for 24 h (n = 4 mice).

(E) Weight loss of HSV-1-infected mice recorded daily (n = 10 mice for each genotype).

Data analyzed by Student's t test (A–D) or two-tailed t test (E) are shown as mean ± SEM, and *p < 0.05, **p < 0.01, ***p < 0.001. UI, uninfected.

See also Figure S7.

under resting conditions and that this transport could be stimulated further by hypotonic cell swelling, cisplatin or GTPγS, or TNF or IL-1. Given that ROS-promoted cysteine oxidation can enhance LRRC8 VRACs (Gradogna et al., 2017; Varela et al., 2004), VRACs may be further activated during viral infection by factors such as TNF, IL-1, or ROS. VRACs transport a broad spectrum of small organic compounds contingent on their LRRC8 subunit composition (Lee et al., 2014; Lutter et al., 2017; Planells-Cases et al., 2015). Whereas LRRC8A complexes with either one of LRRC8B–E to conduct $Cl^-$ efflux, inclusion of

LRRC8D enabled the transport of all investigated organic compounds (Lutter et al., 2017). Our results indicate that LRRC8A/E-containing VRACs are particularly important for the transport of cGAMP and CDNs. Although the principles governing the substrate specificity of LRRC8 channels remain unclear, it is noteworthy that negatively charged aspartate could not only be transported by LRRC8D-containing VRACs but also by VRACs containing LRRC8E or LRRC8C (Lutter et al., 2017; Schober et al., 2017). The fact that cGAMP is negatively charged points to a more general role of LRRC8E-containing VRACs in transporting negatively charged compounds. The relative expression of LRRC8B, -C, -D, -E, as well as cell-intrinsic regulatory networks, likely influence cell type-specific roles of VRAC and the importance of specific LRRC8 subunits in cGAMP transport.

Being channels, VRACs transport substrates by passive diffusion along their electrochemical gradients. Hence, they may mediate both cellular efflux and uptake of cGAMP. This concept is supported by our observation that more cGAMP was exported by HSV-infected WT cells than *Lrrc8a*$^{-/-}$ cells. The negative charges of cGAMP, together with the concentration gradient, would provide a driving force for cGAMP exit from cells. Likewise, under appropriate cGAMP concentration gradients, VRACs can mediate cGAMP uptake as demonstrated by equilibrium potential calculations (data not shown). Conceivably, other mechanisms of cGAMP release might also come into play during HSV-1 infection, including Slc19a1 and RIP3-MLKL-mediated formation of pro-necrotic pores (Su et al., 2014; Wang et al., 2014).

The role of LRRC8 VRACs in immunity may extend well beyond infections with DNA viruses. Being capable of transporting bacterial CDNs, VRACs may also play a role in shaping immune responses against bacterial pathogens. Tumor-derived cGAMP can be transported into host cells, where it elicits IFN response to augment natural killer cell activation (Marcus et al., 2018). Hence, it is tempting to speculate that VRAC-mediated cGAMP efflux and/or influx might also have a role in these processes. Our work suggests that it might be worthwhile to test the role of VRACs in vaccination and explore the possibility of using VRAC agonists as co-adjuvant for cGAMP in cancer vaccine.

In conclusion, we found a role for LRRC8/VRAC-mediated cGAMP transmission in host defense, likely by alerting distant bystander cells to trigger an effective anti-viral IFN response. The demonstration of an interplay between cell volume regulation and innate immune response and the cooperation among infected cells and non-infected cells in host defense may have profound implications in infection, cancer, and vaccine development.

## STAR★METHODS

Detailed methods are provided in the online version of this paper and include the following:

- KEY RESOURCES TABLE
- RESOURCE AVAILABILITY
  - Lead Contact
  - Materials Availability
  - Data and Code Availability
- EXPERIMENTAL MODEL AND SUBJECT DETAILS
  - Mice
  - Peritoneal Macrophages
  - Bone Marrow-derived Macrophages (BMDMs)
  - Mouse Lung Fibroblasts (MLFs)
  - Mouse Embryonic Fibroblasts (MEFs)
  - Cell Culture
- METHOD DETAILS
  - LC-MS/MS Quantification of cGAMP
  - Quantification of cGAMP by ELISA or Functional Assay
  - ELISA Assay
  - Hypotonicity-induced Cell Swelling
  - Transwell Assay
  - siRNA Design and Transfection
  - Gene Targeting with CRISPR-Cas9 in L929 Cells
  - RNA Preparation and Real-Time (RT)-PCR
  - Viral Infection and Plaque Assay
  - Confocal Fluorescence Microscopy
  - Electrophysiology
- QUANTIFICATION AND STATISTICAL ANALYSIS

## SUPPLEMENTAL INFORMATION

Supplemental Information can be found online at https://doi.org/10.1016/j.immuni.2020.03.016.

## ACKNOWLEDGMENTS

This study was supported by the Key Development and Research project 2016YFA0502100 of China; the National Natural Science Foundation of China (81720108019, 81725004, and 31700784), China; the Key Cooperation Program of International Partnership Program (153831KYSB20180003), the Strategic Priority Research Program (XDB29030302), and the External Cooperation Program (153211KYSB20160001) of the Chinese Academy of Sciences, China; the Shanghai Municipal Science and Technology Major Project (2019SHZDZX02), Shanghai, China; the Joint Research grant with State Key Laboratory of Microbial Metabolism, School of Life Science and Biotechnology, Shanghai Jiao Tong University (MMLKF16-11 to C.P.), Shanghai, China; the European Research Council Advanced Grant 740537 (VolSignal) to T.J.J., European Union; and the Klingenstein-Simons Fellowship in Neuroscience and the Sloan Research Fellowship to Z.Q., USA.

## AUTHOR CONTRIBUTIONS

C.Z., X.C., and H.X. conceived and designed the research; C.Z., X.C., R.P.-C., J.C., L.W., L.C., Z.L., K.I.L.-C., Y.X., S.Y., T.L., X.W., F.U., S.M., and Y.F. performed experiments; X.Z., Z.Q., X.L., S.C., Z.J., Q.L., D.Z., T.S.X., K.L., J.Y., H.L., and C.P. provided materials and technical support; Z.Q., T.J.J., and H.X. supervised the study; C.Z., X.C., Z.Q., T.J.J., and H.X. wrote the paper.

## DECLARATION OF INTERESTS

The authors declare no competing interests.

Received: December 19, 2019
Revised: February 24, 2020
Accepted: March 24, 2020
Published: April 10, 2020

## REFERENCES

Ablasser, A., and Chen, Z.J. (2019). cGAS in action: Expanding roles in immunity and inflammation. Science *363*, https://doi.org/10.1126/science.aat8657.

Ablasser, A., and Hur, S. (2020). Regulation of cGAS- and RLR-mediated immunity to nucleic acids. Nat. Immunol. *21*, 17–29.

Ablasser, A., Goldeck, M., Cavlar, T., Deimling, T., Witte, G., Röhl, I., Hopfner, K.P., Ludwig, J., and Hornung, V. (2013a). cGAS produces a 2′-5′-linked cyclic dinucleotide second messenger that activates STING. Nature *498*, 380–384.

Ablasser, A., Schmid-Burgk, J.L., Hemmerling, I., Horvath, G.L., Schmidt, T., Latz, E., and Hornung, V. (2013b). Cell intrinsic immunity spreads to bystander cells via the intercellular transfer of cGAMP. Nature *503*, 530–534.

Barber, G.N. (2015). STING: infection, inflammation and cancer. Nat. Rev. Immunol. *15*, 760–770.

Benfenati, V., Caprini, M., Nicchia, G.P., Rossi, A., Dovizio, M., Cervetto, C., Nobile, M., and Ferroni, S. (2009). Carbenoxolone inhibits volume-regulated anion conductance in cultured rat cortical astroglia. Channels (Austin) *3*, 323–336.

Best, L., Brown, P.D., Sener, A., and Malaisse, W.J. (2010). Electrical activity in pancreatic islet cells: The VRAC hypothesis. Islets *2*, 59–64.

Bridgeman, A., Maelfait, J., Davenne, T., Partridge, T., Peng, Y., Mayer, A., Dong, T., Kaever, V., Borrow, P., and Rehwinkel, J. (2015). Viruses transfer the antiviral second messenger cGAMP between cells. Science *349*, 1228–1232.

Caldwell, J.H., Van Brunt, J., and Harold, F.M. (1986). Calcium-dependent anion channel in the water mold, Blastocladiella emersonii. J. Membr. Biol. *89*, 85–97.

Chen, Q., Boire, A., Jin, X., Valiente, M., Er, E.E., Lopez-Soto, A., Jacob, L., Patwa, R., Shah, H., Xu, K., et al. (2016a). Carcinoma-astrocyte gap junctions promote brain metastasis by cGAMP transfer. Nature *533*, 493–498.

Chen, Q., Sun, L., and Chen, Z.J. (2016b). Regulation and function of the cGAS-STING pathway of cytosolic DNA sensing. Nat. Immunol. *17*, 1142–1149.

Christensen, M.H., Jensen, S.B., Miettinen, J.J., Luecke, S., Prabakaran, T., Reinert, L.S., Mettenleiter, T., Chen, Z.J., Knipe, D.M., Sandri-Goldin, R.M., et al. (2016). HSV-1 ICP27 targets the TBK1-activated STING signalsome to inhibit virus-induced type I IFN expression. EMBO J. *35*, 1385–1399.

Danilchanka, O., and Mekalanos, J.J. (2013). Cyclic dinucleotides and the innate immune response. Cell *154*, 962–970.

Decher, N., Lang, H.J., Nilius, B., Brüggemann, A., Busch, A.E., and Steinmeyer, K. (2001). DCPIB is a novel selective blocker of I(Cl,swell) and prevents swelling-induced shortening of guinea-pig atrial action potential duration. Br. J. Pharmacol. *134*, 1467–1479.

Deng, Z., Ma, S., Zhou, H., Zang, A., Fang, Y., Li, T., Shi, H., Liu, M., Du, M., Taylor, P.R., et al. (2015). Tyrosine phosphatase SHP-2 mediates C-type lectin receptor-induced activation of the kinase Syk and anti-fungal TH17 responses. Nat. Immunol. *16*, 642–652.

Du, M., Liu, J., Chen, X., Xie, Y., Yuan, C., Xiang, Y., Sun, B., Lan, K., Chen, M., James, S.J., et al. (2015). Casein kinase II controls TBK1/IRF3 activation in IFN response against viral infection. J. Immunol. *194*, 4477–4488.

Friard, J., Tauc, M., Cougnon, M., Compan, V., Duranton, C., and Rubera, I. (2017). Comparative Effects of Chloride Channel Inhibitors on LRRC8/VRAC-Mediated Chloride Conductance. Front. Pharmacol. *8*, 328.

Gao, D., Li, T., Li, X.D., Chen, X., Li, Q.Z., Wight-Carter, M., and Chen, Z.J. (2015). Activation of cyclic GMP-AMP synthase by self-DNA causes autoimmune diseases. Proc. Natl. Acad. Sci. USA *112*, E5699–E5705.

Gentili, M., Kowal, J., Tkach, M., Satoh, T., Lahaye, X., Conrad, C., Boyron, M., Lombard, B., Durand, S., Kroemer, G., et al. (2015). Transmission of innate immune signaling by packaging of cGAMP in viral particles. Science *349*, 1232–1236.

Gentili, M., Lahaye, X., Nadalin, F., Nader, G.P.F., Lombardi, E.P., Herve, S., De Silva, N.S., Rookhuizen, D.C., Zueva, E., Goudot, C., et al. (2019). The N-Terminal Domain of cGAS Determines Preferential Association with Centromeric DNA and Innate Immune Activation in the Nucleus. Cell Rep. *26*, 3798.

Gradogna, A., Gavazzo, P., Boccaccio, A., and Pusch, M. (2017). Subunit-dependent oxidative stress sensitivity of LRRC8 volume-regulated anion channels. J. Physiol. *595*, 6719–6733.

Hoffmann, E.K., Lambert, I.H., and Pedersen, S.F. (2009). Physiology of cell volume regulation in vertebrates. Physiol. Rev. *89*, 193–277.

Holmgren, A.M., McConkey, C.A., and Shin, S. (2017). Outrunning the Red Queen: bystander activation as a means of outpacing innate immune subversion by intracellular pathogens. Cell. Mol. Immunol. *14*, 14–21.

Huaux, F., Liu, T., McGarry, B., Ullenbruch, M., and Phan, S.H. (2003). Dual roles of IL-4 in lung injury and fibrosis. J. Immunol. *170*, 2083–2092.

Ishikawa, H., and Barber, G.N. (2008). STING is an endoplasmic reticulum adaptor that facilitates innate immune signalling. Nature *455*, 674–678.

Ishikawa, H., Ma, Z., and Barber, G.N. (2009). STING regulates intracellular DNA-mediated, type I interferon-dependent innate immunity. Nature *461*, 788–792.

Jentsch, T.J. (2016). VRACs and other ion channels and transporters in the regulation of cell volume and beyond. Nat. Rev. Mol. Cell Biol. *17*, 293–307.

Kang, C., Xie, L., Gunasekar, S.K., Mishra, A., Zhang, Y., Pai, S., Gao, Y., Kumar, A., Norris, A.W., Stephens, S.B., and Sah, R. (2018). SWELL1 is a glucose sensor regulating β-cell excitability and systemic glycaemia. Nat. Commun. *9*, 367.

Kono, Y., Nishiuma, T., Nishimura, Y., Kotani, Y., Okada, T., Nakamura, S., and Yokoyama, M. (2007). Sphingosine kinase 1 regulates differentiation of human and mouse lung fibroblasts mediated by TGF-beta1. Am. J. Respir. Cell Mol. Biol. *37*, 395–404.

Kumar, L., Chou, J., Yee, C.S., Borzutzky, A., Vollmann, E.H., von Andrian, U.H., Park, S.Y., Hollander, G., Manis, J.P., Poliani, P.L., and Geha, R.S. (2014). Leucine-rich repeat containing 8A (LRRC8A) is essential for T lymphocyte development and function. J. Exp. Med. *211*, 929–942.

Lai, W.S., Parker, J.S., Grissom, S.F., Stumpo, D.J., and Blackshear, P.J. (2006). Novel mRNA targets for tristetraprolin (TTP) identified by global analysis of stabilized transcripts in TTP-deficient fibroblasts. Mol. Cell. Biol. *26*, 9196–9208.

Lam, E., Stein, S., and Falck-Pedersen, E. (2014). Adenovirus detection by the cGAS/STING/TBK1 DNA sensing cascade. J. Virol. *88*, 974–981.

Lee, C.C., Freinkman, E., Sabatini, D.M., and Ploegh, H.L. (2014). The protein synthesis inhibitor blasticidin s enters mammalian cells via leucine-rich repeat-containing protein 8D. J. Biol. Chem. *289*, 17124–17131.

Li, F., Han, X., Li, F., Wang, R., Wang, H., Gao, Y., Wang, X., Fang, Z., Zhang, W., Yao, S., et al. (2015). LKB1 Inactivation Elicits a Redox Imbalance to Modulate Non-small Cell Lung Cancer Plasticity and Therapeutic Response. Cancer Cell *27*, 698–711.

Liu, H., Moura-Alves, P., Pei, G., Mollenkopf, H.J., Hurwitz, R., Wu, X., Wang, F., Liu, S., Ma, M., Fei, Y., et al. (2019). cGAS facilitates sensing of extracellular cyclic dinucleotides to activate innate immunity. EMBO Rep. *20*, https://doi.org/10.15252/embr.201846293.

Lück, J.C., Puchkov, D., Ullrich, F., and Jentsch, T.J. (2018). LRRC8/VRAC anion channels are required for late stages of spermatid development in mice. J. Biol. Chem. *293*, 11796–11808.

Luo, W.W., Li, S., Li, C., Lian, H., Yang, Q., Zhong, B., and Shu, H.B. (2016). iRhom2 is essential for innate immunity to DNA viruses by mediating trafficking and stability of the adaptor STING. Nat. Immunol. *17*, 1057–1066.

Luteijn, R.D., Zaver, S.A., Gowen, B.G., Wyman, S.K., Garelis, N.E., Onia, L., McWhirter, S.M., Katibah, G.E., Corn, J.E., Woodward, J.J., and Raulet, D.H. (2019). SLC19A1 transports immunoreactive cyclic dinucleotides. Nature *573*, 434–438.

Lutter, D., Ullrich, F., Lueck, J.C., Kempa, S., and Jentsch, T.J. (2017). Selective transport of neurotransmitters and modulators by distinct volume-regulated LRRC8 anion channels. J. Cell Sci. *130*, 1122–1133.

Ma, S., Wan, X., Deng, Z., Shi, L., Hao, C., Zhou, Z., Zhou, C., Fang, Y., Liu, J., Yang, J., et al. (2017). Epigenetic regulator CXXC5 recruits DNA demethylase Tet2 to regulate TLR7/9-elicited IFN response in pDCs. J. Exp. Med. *214*, 1471–1491.

Marcus, A., Mao, A.J., Lensink-Vasan, M., Wang, L., Vance, R.E., and Raulet, D.H. (2018). Tumor-Derived cGAMP Triggers a STING-Mediated Interferon Response in Non-tumor Cells to Activate the NK Cell Response. Immunity *49*, 754–763.e4.

Margolis, S.R., Wilson, S.C., and Vance, R.E. (2017). Evolutionary Origins of cGAS-STING Signaling. Trends Immunol. *38*, 733–743.

Nilius, B., Voets, T., Prenen, J., Barth, H., Aktories, K., Kaibuchi, K., Droogmans, G., and Eggermont, J. (1999). Role of Rho and Rho kinase in the activation of volume-regulated anion channels in bovine endothelial cells. J. Physiol. *516*, 67–74.

Osei-Owusu, J., Yang, J., Vitery, M.D.C., and Qiu, Z. (2018). Molecular Biology and Physiology of Volume-Regulated Anion Channel (VRAC). Curr. Top. Membr. *81*, 177–203.

Pan, D., Han, T., Tang, S., Xu, W., Bao, Q., Sun, Y., Xuan, B., and Qian, Z. (2018). Murine Cytomegalovirus Protein pM91 Interacts with pM79 and Is Critical for Viral Late Gene Expression. J. Virol. *92*, https://doi.org/10.1128/JVI.00675-18.

Pedersen, S.F., Okada, Y., and Nilius, B. (2016). Biophysics and Physiology of the Volume-Regulated Anion Channel (VRAC)/Volume-Sensitive Outwardly Rectifying Anion Channel (VSOR). Pflugers Arch. *468*, 371–383.

Planells-Cases, R., Lutter, D., Guyader, C., Gerhards, N.M., Ullrich, F., Elger, D.A., Kucukosmanoglu, A., Xu, G., Voss, F.K., Reincke, S.M., et al. (2015). Subunit composition of VRAC channels determines substrate specificity and cellular resistance to Pt-based anti-cancer drugs. EMBO J. *34*, 2993–3008.

Platt, C.D., Chou, J., Houlihan, P., Badran, Y.R., Kumar, L., Bainter, W., Poliani, P.L., Perez, C.J., Dent, S.Y., Clapham, D.E., et al. (2017). Leucine-rich repeat containing 8A (LRRC8A)-dependent volume-regulated anion channel activity is dispensable for T-cell development and function. J Allergy Clin Immunol *140*, 1651–1659.e1.

Qiu, Z., Dubin, A.E., Mathur, J., Tu, B., Reddy, K., Miraglia, L.J., Reinhardt, J., Orth, A.P., and Patapoutian, A. (2014). SWELL1, a plasma membrane protein, is an essential component of volume-regulated anion channel. Cell *157*, 447–458.

Ritchie, C., Cordova, A.F., Hess, G.T., Bassik, M.C., and Li, L. (2019). SLC19A1 Is an Importer of the Immunotransmitter cGAMP. Mol. Cell *75*, 372–381.e5.

Roers, A., Hiller, B., and Hornung, V. (2016). Recognition of Endogenous Nucleic Acids by the Innate Immune System. Immunity *44*, 739–754.

Schober, A.L., Wilson, C.S., and Mongin, A.A. (2017). Molecular composition and heterogeneity of the LRRC8-containing swelling-activated osmolyte channels in primary rat astrocytes. J. Physiol. *595*, 6939–6951.

Stempel, M., Chan, B., Juranić Lisnić, V., Krmpotić, A., Hartung, J., Paludan, S.R., Füllbrunn, N., Lemmermann, N.A., and Brinkmann, M.M. (2019). The herpesviral antagonist m152 reveals differential activation of STING-dependent IRF and NF-κB signaling and STING's dual role during MCMV infection. EMBO J. *38*, https://doi.org/10.15252/embj.2018100983.

Stuhlmann, T., Planells-Cases, R., and Jentsch, T.J. (2018). LRRC8/VRAC anion channels enhance β-cell glucose sensing and insulin secretion. Nat. Commun. *9*, 1974.

Su, L., Quade, B., Wang, H., Sun, L., Wang, X., and Rizo, J. (2014). A plug release mechanism for membrane permeation by MLKL. Structure *22*, 1489–1500.

Sun, W., Li, Y., Chen, L., Chen, H., You, F., Zhou, X., Zhou, Y., Zhai, Z., Chen, D., and Jiang, Z. (2009). ERIS, an endoplasmic reticulum IFN stimulator, activates innate immune signaling through dimerization. Proc. Natl. Acad. Sci. USA *106*, 8653–8658.

Sun, L., Wu, J., Du, F., Chen, X., and Chen, Z.J. (2013). Cyclic GMP-AMP synthase is a cytosolic DNA sensor that activates the type I interferon pathway. Science *339*, 786–791.

Varela, D., Simon, F., Riveros, A., Jørgensen, F., and Stutzin, A. (2004). NAD(P)H oxidase-derived H(2)O(2) signals chloride channel activation in cell volume regulation and cell proliferation. J. Biol. Chem. *279*, 13301–13304.

Voets, T., Manolopoulos, V., Eggermont, J., Ellory, C., Droogmans, G., and Nilius, B. (1998). Regulation of a swelling-activated chloride current in bovine endothelium by protein tyrosine phosphorylation and G proteins. J. Physiol. *506*, 341–352.

Voss, F.K., Ullrich, F., Münch, J., Lazarow, K., Lutter, D., Mah, N., Andrade-Navarro, M.A., von Kries, J.P., Stauber, T., and Jentsch, T.J. (2014). Identification of LRRC8 heteromers as an essential component of the volume-regulated anion channel VRAC. Science *344*, 634–638.

Wang, X., Li, Y., Liu, S., Yu, X., Li, L., Shi, C., He, W., Li, J., Xu, L., Hu, Z., et al. (2014). Direct activation of RIP3/MLKL-dependent necrosis by herpes simplex virus 1 (HSV-1) protein ICP6 triggers host antiviral defense. Proc. Natl. Acad. Sci. USA *111*, 15438–15443.

Wilson, C.S., Bach, M.D., Ashkavand, Z., Norman, K.R., Martino, N., Adam, A.P., and Mongin, A.A. (2019). Metabolic constraints of swelling-activated glutamate release in astrocytes and their implication for ischemic tissue damage. J. Neurochem. *151*, 255–272.

Wu, J., Sun, L., Chen, X., Du, F., Shi, H., Chen, C., and Chen, Z.J. (2013). Cyclic GMP-AMP is an endogenous second messenger in innate immune signaling by cytosolic DNA. Science *339*, 826–830.

Yang, J., Vitery, M.D.C., Chen, J., Osei-Owusu, J., Chu, J., and Qiu, Z. (2019). Glutamate-Releasing SWELL1 Channel in Astrocytes Modulates Synaptic Transmission and Promotes Brain Damage in Stroke. Neuron *102*, 813–827.e6.

Zhong, B., Yang, Y., Li, S., Wang, Y.Y., Li, Y., Diao, F., Lei, C., He, X., Zhang, L., Tien, P., and Shu, H.B. (2008). The adaptor protein MITA links virus-sensing receptors to IRF3 transcription factor activation. Immunity *29*, 538–550.

Zhou, Y., Fei, M., Zhang, G., Liang, W.C., Lin, W., Wu, Y., Piskol, R., Ridgway, J., McNamara, E., Huang, H., et al. (2020). Blockade of the Phagocytic Receptor MerTK on Tumor-Associated Macrophages Enhances P2X7R-Dependent STING Activation by Tumor-Derived cGAMP. Immunity *52*, 357–373.e9.

## STAR★METHODS

### KEY RESOURCES TABLE

| REAGENT or RESOURCE | SOURCE | IDENTIFIER |
|---|---|---|
| Antibodies | | |
| Rabbit anti-pIRF3 (Ser396 clone 4D4G) | Cell Signaling Technology | Cat# 4947; RRID: AB_823547 |
| Rabbit anti-IRF3 (clone D83B9) | Cell Signaling Technology | Cat# 4302; RRID: AB_1904036 |
| Rabbit anti-pTBK1 (Ser172 clone D52C2) | Cell Signaling Technology | Cat# 5483; RRID: AB_10693472 |
| Rabbit anti-TBK1 (clone D1B4) | Cell Signaling Technology | Cat# 3504; RRID: AB_2255663 |
| Rabbit anti-STING (clone D2P2F) | Cell Signaling Technology | Cat# 13647; RRID: AB_2732796 |
| Rabbit anti-pSTING (Ser365 clone D8F4W) | Cell Signaling Technology | Cat# 72971; RRID: AB_2799831 |
| Rabbit anti-STAT1 | Cell Signaling Technology | Cat# 9172S; RRID: AB_2198300 |
| Rabbit anti-pSTAT1 (Tyr701clone D4A7) | Cell Signaling Technology | Cat# 9171; RRID: AB_331591 |
| Rabbit anti-GAPDH | Bioworld | Cat# AP0063; RRID: AB_2651132 |
| Rabbit Anti-LRRC8A | Laboratories of Thomas J. Jentsch and Zhaozhu Qiu | Voss et al., 2014; Yang et al., 2019 |
| Rabbit Anti-LRRC8B | Laboratory of Thomas J. Jentsch | Stuhlmann et al., 2018 |
| Rabbit Anti-LRRC8C | Laboratory of Thomas J. Jentsch | Stuhlmann et al., 2018 |
| Rabbit Anti-LRRC8D | Laboratory of Thomas J. Jentsch | Stuhlmann et al., 2018 |
| Rabbit Anti-LRRC8E | Laboratory of Thomas J. Jentsch | Stuhlmann et al., 2018 |
| Bacterial and Virus Strains | | |
| HSV-1 KOS strain | Laboratory of Xiaozheng Liang | Du et al., 2015 |
| HSV-GFP | Laboratory of Xiaozheng Liang | Ma et al., 2017 |
| VSV Indiana strain | Laboratory of Xiaozheng Liang | Ma et al., 2017 |
| Adeno-virus-GFP | Laboratory of Hongbin Ji | Li et al., 2015 |
| MCMV BAC pSMgfp | Laboratory of Zhikang Qian | Pan et al., 2018 |
| Biological Samples | | |
| Bone Marrow from BMDMs | This paper; | N/A |
| Embryos from mice for MEFs | This paper; | N/A |
| Lungs from mice for MLFs | This paper; | N/A |
| Chemicals, Peptides, and Recombinant Proteins | | |
| 2′3′-cGAMP | InvivoGen | Cat# tlrl-nacga23-5 |
| 3′3′-cGAMP | InvivoGen | Cat# tlrl-nacga |
| c-di-AMP | InvivoGen | Cat# tlrl-nacda |
| c-di-GMP | InvivoGen | Cat# tlrl-nacdg |
| polyI:C | InvivoGen | Cat# tlrl-picw |
| LPS | InvivoGen | Cat# tlrl-eklps |
| LIPOFECTAMINE 2000 REAGENT | Thermo Fisher | Cat# 1668019 |
| Lipofectamine RNAiMAX Transfection Reagent | Thermo Fisher | Cat# 13778030 |
| Digitonin | Sigma Aldrich | Cat# D141-100MG |
| Carbenoxolone | TOCRIS | Cat# 3096 |
| DCPIB | TOCRIS | Cat# 1540 |
| CaCCinh-A01 | TOCRIS | Cat# 4877 |
| DIDS | TOCRIS | Cat# 4523 |
| Glibenclamide | TOCRIS | Cat# 0911 |
| Cisplatin | TOCRIS | Cat# G2251 |
| Tamoxifen | Sigma Aldrich | Cat# T5648 |
| TRIzol | Thermo Fisher | Cat# 15596026 |

(*Continued on next page*)

*Continued*

| REAGENT or RESOURCE | SOURCE | IDENTIFIER |
|---|---|---|
| Guanosine 5′-[γ-thio] triphosphate tetralithium salt | Sigma Aldrich | Cat# G8634 |
| Phosphodiesterase I from Crotalus adamanteus venom | Sigma Aldrich | Cat# P3134 |
| PMA–Phorbol 12-myristate 13-acetate | SIGMA | Cat# P8139 |
| DMXAA | Selleck Chemicals | Cat# S1537 |
| Critical Commercial Assays | | |
| LEGEND MAX™ Mouse IFN-β ELISA Kit | biolegend | Cat# 439408 |
| Murine IP-10 ELISA Development Kit | Peprotech | Cat# 900-K153 |
| Murine Rantes ELISA Development Kit | Peprotech | Cat# 900-K124 |
| Mouse TNF-alpha ELISA Ready-SET-Go! Set 10 plates | eBioscience | Cat# 8-7324-88 |
| Lonza MycoAlert Mycoplasma Detection Kit | Lonza | Cat# LT07-418 |
| LDH-Glo™ Cytotoxicity Assay | Promega | Cat# J2380 |
| 2′3′-cGAMP ELISA Kit | Cayman | Cat# 501700 |
| 6-well Transwell with 0.4μm pores | Corning | Cat# 3450 |
| Hyper Sep Aminopropyl SPE Columns | Thermo Fisher | Cat# 60108-364 |
| Deposited Data | | |
| Complete, uncropped western blots | This paper, and Mendeley Data | https://data.mendeley.com/datasets/ss37r6d45n/1 |
| Experimental Models: Cell Lines | | |
| human HEK293T cells | ATCC | ATCC CRL-3216; RRID: CVCL_0063 |
| human HEK293 cells | ATCC | ATCC CRL-1573; RRID: CVCL_0045 |
| Mouse fibroblasts L929 | ATCC | ATCC CCL-1; RRID: CVCL_0462 |
| Human THP-1 cells | ATCC | ATCC TIB-202; RRID: CVCL_0006 |
| HeLa WT | Laboratory of Zhaozhu Qiu | Yang et al., 2019 |
| HeLa *LRRC8A*$^{-/-}$ | Laboratory of Zhaozhu Qiu | Yang et al., 2019 |
| L929 *Sting*$^{-/-}$ | This paper | N/A |
| L929 *Cgas*$^{-/-}$ | This paper | N/A |
| L929 *Lrrc8a*$^{-/-}$ | This paper | N/A |
| L929 *Lrrc8e*$^{-/-}$ | This paper | N/A |
| MEF *Sting*$^{-/-}$ | This paper | N/A |
| MEF *Cgas*$^{-/-}$ | This paper | N/A |
| MEF *Lrrc8a*$^{-/-}$ | This paper | N/A |
| MEF *Lrrc8e*$^{-/-}$ | This paper | N/A |
| BMDM WT | This paper | N/A |
| BMDM *Lrrc8a*$^{-/-}$ | This paper | N/A |
| BMDM *Lrrc8e*$^{-/-}$ | This paper | N/A |
| MLF WT | This paper | N/A |
| MLF *Lrrc8a*$^{-/-}$ | This paper | N/A |
| MLF *Lrrc8b*$^{-/-}$ | This paper | N/A |
| MLF *Lrrc8c*$^{-/-}$ | This paper | N/A |
| MLF *Lrrc8d*$^{-/-}$ | This paper | N/A |
| MLF *Lrrc8e*$^{-/-}$ | This paper | N/A |
| Experimental Models: mice/Strains | | |
| C57BL/6N WT mice | Jackson Laboratory | Stock# 005304 |
| C57BL/6N-*Lrrc8b*$^{-/-}$ mice | This paper | N/A |
| C57BL/6N-*Lrrc8c*$^{-/-}$ mice | This paper | N/A |
| C57BL/6N-*Lrrc8d*$^{-/-}$ mice | This paper | N/A |
| C57BL/6N-*Lrrc8e*$^{-/-}$ mice | This paper | N/A |
| C57BL/6N-*Lrrc8a*$^{f/f}$ mice | Laboratory of Zhaozhu Qiu | Yang et al., 2019 |

(*Continued on next page*)

| Continued | | |
|---|---|---|
| REAGENT or RESOURCE | SOURCE | IDENTIFIER |
| C57BL/6N-*Lrrc8a*$^{f/f:creERT}$ mice | This paper | N/A |
| C57BL/6N-*Lrrc8e*$^{-/-}$ mice | This paper | N/A |
| C57BL/6J-*Sting*$^{-/-}$ mice | Jackson Laboratory | Stock# 017537 |
| C57BL/6J WT mice | Jackson Laboratory | Stock# 000664 |
| C57BL/6-*Cgas*$^{-/-}$ mice | Jackson Laboratory | Stock# 026554 |
| Oligonucleotides | | |
| See Table S1 for oligonucleotides for SgRNAs, SiRNAs, RT-PCRs. | This paper | N/A |
| Recombinant DNA | | |
| pIP-FLAG-Lrrc8a | This paper | N/A |
| pIP-HA-Lrrc8a | This paper | N/A |
| pIP-FLAG-Lrrc8e | This paper | N/A |
| pIP-HA-Lrrc8e | This paper | N/A |
| PCDNA3.1-FLAG-cGAS | This paper | N/A |
| pLVX-N-mCherry-hSTING | This paper | N/A |
| lentiCRISPR v2 | Addgene plasmid | Addgene 52961; RRID: Addgene_52961 |
| pLentiCRISPR plasmid | Addgene plasmid | Addgene 78852; RRID: Addgene_ 78852 |
| Software and Algorithms | | |
| GraphPad Prism 7.01 | GraphPad Software | https://www.graphpad.com/scientific-software/prism/ |
| ImageJ (v. 2.0.0-rc-43/1.51k) | | https://imagej.nih.gov/ij/index.html |

## RESOURCE AVAILABILITY

### Lead Contact

Further information and requests for resources and reagents should be directed to and will be fulfilled by the Lead Contact, Hui Xiao (huixiao@ips.ac.cn).

### Materials Availability

There is no restriction to the availability of reagents/materials generated in this study.

### Data and Code Availability

Original/source data for figures in the paper is available [Mendeley Data https://doi.org/10.17632/ss37r6d45n.1].

## EXPERIMENTAL MODEL AND SUBJECT DETAILS

### Mice

All Lrrc8 VRAC-deficient mice were on C57BL/6N background, and both male and female littermates were used for all the experiments. *Lrrc8a*/*Swell1*$^{f/f}$ mice (on C57BL6 background) were generated and described previously (Yang et al., 2019). Briefly, mouse embryonic stem (ES) cells bearing a floxed *Lrrc8a* allele from the European Conditional Mouse Mutagenesis Program (EUCOMM) were used to generate chimeric mice by blastocyst injection. *Lrrc8a*$^{f/f}$ mice were bred onto Rosa26-creERT2 (B6/129) mouse strain (from Jackson Labs) to generate *Lrrc8a*$^{f/f:creERT}$ mouse in this study. *Lrrc8e*$^{-/-}$ mice were generated at the Leibniz-Forschungsinstitut für Molekulare Pharmakologie (FMP), Berlin. *Lrrc8b*$^{-/-}$, *Lrrc8c*$^{-/-}$, *Lrrc8d*$^{-/-}$ and *Lrrc8e*$^{-/-}$ (STY-051) mice were generated by Biocytogen in Beijing, China using the sgRNAs listed in Table S1. The *Sting*$^{-/-}$ and *Cgas*$^{-/-}$ mice on C57B/6J background were from the Jackson Labs. All the mice were bred and maintained in a pathogen-free animal facility at Institut Pasteur of Shanghai. All procedures were conducted in compliance with a protocol approved by the Institutional Animal Care and Use Committee at Institut Pasteur of Shanghai.

### Peritoneal Macrophages

Peritoneal macrophages were isolated from 6- to 8-weeks-old C57BL/6J mice. 3 days after intraperitoneal injection of 2 mL of 3% thioglycollate medium (BD, Cat#: 211716), peritoneal macrophages were isolated and cultured in RPMI 1640 medium supplemented with 10% FBS (HyClone, Cat#: SH30084.03), 100 U/mL penicillin, and 100 mg/mL streptomycin for use.

### Bone Marrow-derived Macrophages (BMDMs)

*Lrrc8a*$^{f/f}$ and *Lrrc8a*$^{f/f:creERT}$ mice (6 weeks of age, sex-matched littermates on C57B6/129 background) were administered tamoxifen (Sigma-Aldrich, Cat#: T5648). 2 mg of tamoxifen in 0.2 mL corn oil was delivered by intraperitoneal injection once every two days, and 3 times in total to induce the deletion of *Lrrc8a*. Primary BMDMs and MLFs were prepared 1 week after the last injection of tamoxifen.

BMDMs were differentiated according to the method described previously (Deng et al., 2015). Bone marrow cells from 8-10 weeks old WT and *Lrrc8e*$^{-/-}$ littermates were cultured in RPMI-1640 medium supplemented with 30% L929 conditioned medium and 10% FBS for 5-7 days before use.

### Mouse Lung Fibroblasts (MLFs)

MLFs were prepared from *Lrrc8a*$^{f/f}$ and *Lrrc8a*$^{f/f:creERT}$ mice injected with 3 doses of tamoxifen as described above or from 8-10 weeks old WT and *Lrrc8b*$^{-/-}$, *Lrrc8c*$^{-/-}$, *Lrrc8d*$^{-/-}$ or *Lrrc8e*$^{-/-}$ littermates using a protocol described previously (Huaux et al., 2003; Kono et al., 2007). Briefly, mouse lungs were cut into small pieces and digested with 0.1% collagenase D and trypsin in serum-free DMEM at 37°C for 1 h. Digested fibroblasts were centrifuged, washed, and then cultured in DMEM containing 10% FBS. In 6-12 h, the non-adherent cells were washed off, and the adherent cells were cultured with DMEM containing 20% FBS, 100 U/mL penicillin and 100 mg/mL streptomycin for 5-10 days.

### Mouse Embryonic Fibroblasts (MEFs)

MEFs were isolated as previously described (Lai et al., 2006). E14.5 embryos were digested overnight with 2 to 3 mL of ice-cold 0.25% trypsin-EDTA at 4°C. After vigorously pipetting, digested cells were dispersed and then spun down. After wash with PBS, embryonic cells were cultured in 10-cm dishes with DMEM containing 20% FBS, 100 U/mL penicillin and 100 mg/mL streptomycin for 5-7 days. When *Lrrc8a*$^{f/f}$ MEF cells reached approximately 70 to 90% confluence, retroviral vectors pCDH or pCDH-Cre were transducted. Following puromycin-selection for 5 days, both WT and *Lrrc8a*$^{-/-}$ MEFs were obtained for experiments.

### Cell Culture

Mouse fibroblasts L929, MEFs, HeLa and human HEK293T and HEK293 (from American Type Culture Collection) were cultured in DMEM (HyClone, Cat#: SH30243.01) supplemented with 10% FBS, 100 U/mL penicillin, and 100 mg/mL streptomycin. Human THP-1 cells (from American Type Culture Collection) were cultured in RPMI 1640 medium (HyClone, Cat#: SH30809.01) supplemented with 10% FBS, 2 mM L-Glutamine, 50 μM 2-mercaptoethanol, 1 mM pyruvic acid, 100 U/mL penicillin, and 100 mg/mL streptomycin. All cell lines were checked monthly for mycoplasma contamination by commercial PCR (Lonza Mycoalert Cat#: LT07-418).

## METHOD DETAILS

### LC-MS/MS Quantification of cGAMP

Cellular cGAMP preparation was performed following previous protocols (Gao et al., 2015; Wu et al., 2013). Briefly, HSV-1-infected or cGAMP-incubated cells were lysed in 1 mL of lysis buffer containing 80% of methanol and 2% of acetic acid pre-chilled to 80°C. After incubation for 5 min on ice, the lysates were centrifuged at 10,000 g for 10 min, and the pellets were extracted with 0.5 mL of 2% acetic acid. The extracted cGAMP was enriched by Hyper Sep Aminopropyl SPE Columns (Thermo Scientific), and eluted with 1 mL of 4% ammonium hydroxide in 80% methanol. Following vacuum dry, the cGAMP was reconstituted in 40 μL of 50% acetonitrile and were ultrasonicated for 15 min at room temperature. After centrifugation at 14,000 rpm for 15 min, the supernatant was collected for LC-MS/MS analysis. The LC-MS/MS analysis was performed on an Agilent 1290 UPLC (Agilent, USA) coupled to an AB Sciex 6500 Triple Quad mass spectrometer (AB Sciex, USA) with the electrospray ionization (ESI) source. A Waters ACQUITY UPLC BEH Amide column (1.7 μm, 2.1 × 100 mm) was used for GAMP separation with a flow rate at 0.4 mL/min and column temperature of 45°C. The mobile phases were comprised of (A) 0.2% formic acid and 10 mM ammonium acetate in 50% acetonitrile and (B) 0.2% formic acid and 10 mM ammonium acetate in 95% acetonitrile. The gradient elution was 80% B kept for 1.0 min, then changed linearly to 5% B during 7.0 min, increased to 80% B in 7.1 min and maintained for 2.9 min. The injection volume was set to 2 μL. The mass parameters were as follows: ion spray voltage was 5500 V, ion source temperature was 500°C, collision gas was Medium, ion source gas 1 was 50 psi, ion source gas 2 was 60 psi, curtain gas was 35 psi. Multiple Reaction Monitoring (MRM) was used to monitor GAMP in the positive ion mode. The proposed assay exhibits a good linear range of 2.5–500 ng/mL (2.5, 5, 10, 25, 50, 100, 250 and 500 ng/mL) for GAMP, which sufficiently covers the typical levels determined in actual samples.

### Quantification of cGAMP by ELISA or Functional Assay

MEFs of various genotypes (5 × $10^4$ cells in total) were seeded on a 48-well plate and infected with HSV-1 (MOI: 5) for 3 h. The supernatant was collected and cGAMP was measured by Cayman Chemical 2'3'-cGAMP ELISA Kit (Interchim, Cat#:501700) according to manufacturer's instruction.

For extracellular cGAMP functional assay, 1 × $10^7$ MEF cells were infected with HSV-1 (MOI: 5) for 3 h, and cell media were collected and centrifuged at 13,000 rpm for 10 min. After discarding insoluble pellets, the supernatants were digested with 1000 U/mL of Benzonase at 37°C for 40 min in the presence or absence of 0.5 U/mL of snake venom PDE (Sigma, isolated from

*Crotalus adamanteus*) (Ablasser et al., 2013b; Bridgeman et al., 2015). Afterward the supernatants were heated at 95°C for 10 min, followed by centrifugation at 13,000 rpm for 10 min, and then added to recipient MEFs of various genotypes for 3 h prior to RNA extraction and real-time PCR analysis of IFN response.

### ELISA Assay

BMDMs, MEFs, and MLFs were infected with various MOIs of HSV-1 or VSV for 16-24 h, or treated with 5-10 μg/mL of 2'3'cGAMP for 12 h. The amounts of IFN-β, CXCL-10, CCL-5 and TNF were assessed with ELISA kits according to the manufacturers' recommendations (CCL-5 ELISA, peprotech Cat#: 900-K124; IP-10 ELISA, peprotech Cat#: 900-K153; IFN-β ELISA, Biolegend Cat#: 439407 and TNF ELISA, Systems from eBioscience).

### Hypotonicity-induced Cell Swelling

Cells were incubated with isotonic buffer (110 mM mannitol, 90 mM NaCl, 2 mM KCl, 1mM $MgCl_2$, 1 mM $CaCl_2$, and 10 mM HEPES, pH 7.4), hypotonic buffer (10 mM mannitol, 90 mM NaCl, 2 mM KCl, 1mM $MgCl_2$, 1 mM $CaCl_2$, and 10 mM HEPES, pH 7.4) or hypertonic buffer (220 mM mannitol, 90 mM NaCl, 2 mM KCl, 1mM $MgCl_2$, 1 mM $CaCl_2$, and 10 mM HEPES, pH 7.4) for 3 h, in the absence or presence of cGAMP.

For chloride-depletion, 90 mM sodium chloride in both isotonic and hypotonic buffer was replaced with 90 mM sodium gluconate.

### Transwell Assay

The upper cells, such as HEK293 cells ($2.5 \times 10^5$ per ml) transiently transfected with either empty vector or cGAS-expressing plasmid (4μg/mL) for 12 h, WT or *Sting*$^{-/-}$ MEFs transfected with dsDNA (8 μg/mL, lipofectamine) for 3 h, or WT or *Sting*$^{-/-}$ MEFs infected with HSV-1 (MOI: 5) for 3 h, were grown on a transwell (6-well Transwell with 0.4 μm pores from Corning, Cat# 3450) before co-culture with the recipient bystander cells. After transfection or infection, the culture media were removed, and the upper cells were washed 2-3 times with PBS prior to co-culture with the recipient cells. The recipient cells, including MEFs and MLFs of various genotypes ($2 \times 10^5$ per ml), were pre-seeded on 6-well culture plates, and grew separately until co-culture with various upper cells in the transwell chamber for another 6 h. In the case of DCPIB treatment, DCPIB (20 μM) was added into the recipient cells 30 min before co-culture, and presented throughout the entire course of co-culture. Subsequently, the transwell chamber was removed and the recipient cells were collected for RNA preparation and RT-PCR analysis for IFN response.

### siRNA Design and Transfection

siRNAs targeting *Lrrc8a-e*, *Cx43*, or *Panx1* were ordered from GenePharma and listed in Table S1. SiRNAs were transfected to cells by Lipofectamine RNAiMAX Transfection Reagent (Thermo Fisher Cat#: 13778030) for 2-3 days before stimulation.

### Gene Targeting with CRISPR-Cas9 in L929 Cells

SgRNAs against *Lrrc8a or Lrrc8e* were designed (https://www.genscript.com/gRNA-design-tool.html) and listed in Table S1. The annealed sgRNA oligos were cloned into pLentiCRISPR plasmid (Addgene #78852), and packaged in HEK293T cells. Viral media were harvested after 50 h. The Lenti-viruses-containing media were passed through a 0.45 μm filter and added to L929 cells under selection with 1.5 mg/mL puromycin (Sigma Aldrich) for 1 week. and puromycin-resistant clones were screened followed by DNA sequencing.

### RNA Preparation and Real-Time (RT)-PCR

Total RNAs were extracted from L929, MEF and THP1 and peritoneal macrophages using TRIzol (Invitrogen, Cat#: 10296010) according to the manufacturer's instruction. cDNA was reversely transcribed from 500 ng total RNA by PrimeScript RT-PCR kit (Takara, Cat#: RR014). RT-PCR was carried out with primer pairs listed in Table S1 on an ABI 7900HT Fast RT-PCR System. Data shown were the relative abundance of the indicated mRNA normalized to that of *Gapdh* by the change-in-cycling-threshold (ΔΔCT) method.

### Viral Infection and Plaque Assay

MEFs, L929 cells and MLFs ($5 \times 10^5$ per ml) were infected with HSV-1 or VSV in serum-free medium for 2 h as described previously (Ma et al., 2017). Afterward, virus-containing medium was removed and replaced with serum-containing DMEM medium. In 12 h post-infection, cells were harvested and RNAs were prepared by TRIzol. To check viral-induced cell death, 1.5 h after viral-infected, the supernatant was removed and cells were overlaid by 2 × MEM containing 1.6% agar. 36 h post infection stained with 0.5% crystal violet dissolved in 4% formaldehyde for 2 h. Viral titers (pfu/mL) were calculated based on counted plaques.

8-weeks old sex-matched littermates on C57BL/6N background were intravenously injected with HSV-1 (KOS strain, $1 \times 10^7$ plaque-forming units PFU) and VSV (Indiana strain, $5 \times 10^6$ pfu) in 0.1 mL PBS (Ma et al., 2017), and the weight-loss of the infected mice was monitored daily up to 10 days. In 24 h post-infection, mouse sera were collected for ELISA, and the organs such as kidney, liver and spleen were removed and homogenized for RNA preparation and real-time PCR analyses.

HSV-1 and VSV plaque assay was performed as described previously (Du et al., 2015; Ma et al., 2017). Briefly, the supernatants harvested from virus-infected cells were serial diluted in serum-free DMEM and then added into confluent Vero cells cultured on

6-well plates. In 1 h, supernatants were removed and cells were overlaid by 4% methylcellulose. Three days later, the overlay medium was removed and cells were fixed with 4% formaldehyde for 1 h and then stained with 0.5% crystal violet. Viral titers (pfu/mL) were calculated based on counted plaques.

### Confocal Fluorescence Microscopy

MEFs were transfected with pLVX-N-mCherry-hSTING by Lipofectamine 2000 Transfection Reagent (Thermo Fisher, Cat#: 11668019) for 12 h. Subsequently, the liposomal/DNA-containing media were removed and transfected cells were infected with Adeno-virus-GFP (MOI: 0.01) or MCMV BAC *pSMgfp* (MOI: 0.01) for 24 h (Adeno-virus-GFP (Li et al., 2015) was kindly provided by Hongbin Ji from Institute of Biochemistry and Cell Biology, Shanghai, China; and MCMV BAC *pSMgfp* (Pan et al., 2018) was kindly provided by Zhikang Qian from Institut Pasteur of Shanghai, China). Next, the virus infected cells or cGAMP-treated cells were fixed with 4% paraformaldehyde for 10 min and stained with DAPI for 5 min at room temperature. The fluorescence images were collected on a laser capture confocal microscope (FV1200, Olympus) using separate laser excitation to avoid any cross-interference between different fluorophores.

### Electrophysiology

Whole-cell patch-clamp recordings were performed as described previously (Yang et al., 2019). HeLa cells were plated onto coverslips 24-48 h before recording. For hypotonicity-activated VRAC current recordings, HeLa or HCT116 cells were whole-cell patched in isotonic bath solution containing (in mM): 50 NaCl, 10 HEPES, 200 mannitol (pH adjusted to pH 7.3 with NaOH and osmolality adjusted to 310 mOsm/kg), then hypotonic solution (HYPO) contains the same ionic composition but with only 100 mannitol were applied. Recording pipettes were pulled by a micropipette puller (P-1000, Sutter instrument) and had a resistance of 5-10 MΩ when filled with the $Cl^-$ based intracellular solution containing (in mM): 50 NaCl, 10 HEPES, 200 mannitol (pH adjusted to pH 7.3 with NaOH and osmolality adjusted to 310 mOsm/kg). $cGAMP^{2-}$ based intracellular solution was made by replacing 50 NaCl and 200 mannitol with 50 $Na_2$cGAMP (from ChemieTek) and 150 mannitol to maintain the same osmolality. Relative permeability of $cGAMP^{2-}$ to $Cl^-$ was estimated based on the reversal potential difference as described previously (Caldwell et al., 1986). The voltage ramp protocol (5 s or 15 s interval, 500 ms or 2.5 s duration) was used with a holding potential of 0 mV and depolarized from −100 to +100 mV. Recordings were made with MultiClamp 700B amplifier and 1550B digitizer (Molecular Device) or an EPC-10 amplifier. Data acquisition were performed with pClamp 10.7 (Molecular Device) or Patchmatser (HEKA) software, filtered at 1 kHz and digitized at 10 kHz.

## QUANTIFICATION AND STATISTICAL ANALYSIS

All data are shown as mean values, and error bars represent SEM from the number of assays indicated (from at least three independent experiments). For statistical comparisons, data were analyzed by an unpaired two-tailed Student's t test (*$p < 0.05$, **$p < 0.01$, ***$p < 0.001$; by Student's t test) to determine differences between groups using Prism software (GraphPad Software).